TÜBİTAK

Turkish Journal of Earth Sciences

http://journals.tubitak.gov.tr/earth/

Research Article

Turkish J Earth Sci
(2021) 30: 161-181

doi:10.3906/yer-2006-23

Earthquake history of the Yatağan Fault (Muğla, SW Turkey): implications for regional seismic hazard assessment and paleoseismology in extensional provinces

Mehran BASMENJI[1,*], Hüsnü Serdar AKYÜZ[1], Erdem KIRKAN[1], Murat Ersen AKSOY[2], Gülsen UÇARKUŞ[1], Nurettin YAKUPOĞLU[1]

[1]Department of Geological Engineering, Faculty of Mines, İstanbul Technical University, İstanbul, Turkey
[2]Department of Geological Engineering, Muğla Sıtkı Koçman University, Muğla, Turkey

Received: 20.06.2020 • **Accepted/Published Online:** 14.11.2020 • **Final Version:** 22.03.2021

Abstract: The southern part of the Western Anatolia Extensional Province is governed by E-W-trending horst-graben systems and NW-SE-oriented active faults. The NW-striking Yatağan Fault is characterised by an almost pure normal sense of motion with a minor dextral strike slip component. Although the settlements within the area have been affected by several earthquake events since ancient times (~2000 BCE), the earthquake potential and history of the Yatağan Fault has remained unknown until a few years ago. Considering the growing dense population within the area, paleoseismology studies were conducted in order to illuminate the historical earthquake activity on the Yatağan Fault. Two trenches were excavated on the fault. Structural and stratigraphic evidence from the both trenches indicated an event horizon of a paleo-earthquake that was dated between 366 and 160 BCE and 342 ± 131 CE. This event horizon most probably reflected the evidence of the latest large earthquake rupture on the Yatağan Fault.

Key words: Yatağan Fault, paleoseismology, active tectonics, western Anatolia

1. Introduction

Paleoseismology is a powerful technique to study the earthquake history and potential of active faults. Previous paleoseismology studies along normal fault systems have provided important information regarding the seismotectonic behaviour, timing, slip rates, size, and intervals of past earthquakes (Pantosti et al., 1993; Altunel et al., 1999; McCalpin and Hart, 2002; Akyüz et al., 2006; McCalpin, 2009; Tsodoulos et al., 2016; Galli et al., 2019).

Morphologic and stratigraphic features generated by normal faulting (extensional environments) can be detected easier than other tectonic settings of compressional or strike-slip faulting (McCalpin, 2009). Surface deformation in extensional tectonic environments are dominantly characterised by vertical displacement and crustal thinning (McCalpin and Hart, 2002; McCalpin, 2009). Evidence of coseismic extensional deformation, produced by normal faults in the upper crust are recorded in stratigraphic units. This evidence comprises important indicators to study the vertical elevation changes and characteristics of past earthquakes (Galli and Bosi, 2002; McCalpin and Hart, 2002; McCalpin, 2009). Therefore, many researchers have studied the stratigraphic and structural characteristics beneath normal fault scarps to understand whether these structures were formed by shallow creeps (Radbruch-Hall, 1978; Varnes et al., 1989; McCalpin and Hart, 2002) or by sudden vertical displacements, as has been observed after several earthquakes around the world, such as in western Turkey, Greece, Italy, etc. (Pantosti et al., 1993; Altunel et al., 1999; Akyüz et al., 2006; Özkaymak et al., 2011; Tsodoulos et al., 2016; Galli et al., 2019). Recorded vertical displacement in stratigraphic units that were generated by normal faulting may indicate large earthquakes. Therefore, the popularity of applying paleoseismology to study the tectonic activity of small normal faults (10–30 km) with relatively low slope rates (e.g.,<1mm/year) that can produce moderate to relatively strong earthquakes has recently increased (Tsodoulos et al., 2016).

Modern paleoseismic studies in extensional regions, such as investigations of the Dinar Fault (Altunel et al., 1999), Çay Segment of the Akşehir Fault (Akyüz et al., 2006), and Manisa Fault Zone (Özkaymak et al., 2011) in Western Turkey; the Gyrtoni Fault in Greece (Tsodoulos et al., 2016); and the Mont Vettore and Irpina faults in Italy (Pantosti et al., 1993; Galadini and Galli, 2003; Galli et al., 2019) have notably suggested that stratigraphic and structural indicators of past earthquake events observed in the trenches were quite similar. Furthermore, previous studies

* Correspondence: basmenji17@itu.edu.tr

have indicated that repeated ground ruptures along active normal faults mostly occur along mountain-piedmont junctions, and fault scarp genesis and geometry are likely to develop in similar ways, largely independent of the climatic conditions of the regions (McCalpin and Hart, 2002; McCalpin, 2009). Moreover, these studies have proven the efficacy of paleoseismology in seismic hazard assessments, particularly for active normal faults that can produce surface ruptures in hundreds to a few thousand years (Galli et al., 2019).

Convergence between the African, Arabian, and Eurasian plates actively deforms a large area, from western Turkey to eastern Iran, and shapes the continental crust within the region (Şengör and Kidd, 1979; Allen et al., 2004; Reilinger et al., 2006; Seyitoğlu et al., 2019). In particular, collision between the Arabian and the Eurasian plates along the Bitlis-Zagros Suture Zone (Figure 1a) has generated compressional forces in the Turkish-Iranian Plateau, where collision-related deformations are accommodated by several intracontinental active fault zones (Şengör and Kidd, 1979; Adamia et al., 1981; Şengör and Yilmaz, 1981; Şengör et al., 1985; Allen et al., 2004; Reilinger et al., 2006; Aktug et al., 2016; Seyitoğlu et al., 2017; Seyitoğlu et al., 2019). These compressional forces led to the westward escape of the Anatolian microplate along the dextral North Anatolian Fault Zone (NAFZ) and sinistral East Anatolian Fault Zone (Şengör, 1980; Allen et al., 2004; Reilinger et al., 2006). This westward escape is accelerated by the pull effect (back-arc spreading) of the Aegean Subduction Zone (McKenzie, 1972; Şengör et al., 1985; DeMets et al., 1990; Oral et al., 1995; Barka and Reilinger, 1997; Reilinger et al., 1997; Bozkurt, 2001).

The current tectonic and kinematic regime of the western part of the Anatolian microplate is governed by the right-lateral NAFZ in the north and Aegean Subduction Zone in the south (McKenzie, 1978; Le Pichon and Angelier, 1979; Le Pichon et al., 1995; Oral et al., 1995; Barka and Reilinger, 1997; McClusky et al., 2003; Reilinger et al., 2006). The Western Anatolian Extensional Province is currently experiencing N-S extension (McClusky et al., 2000; Reilinger et al., 2006). Toward the SW of this region, the total extension is distributed between E-W-trending Büyük Menderes Graben and the Gökova Fault Zone. The Aegean Arc-Trench System dominantly controls the evolution of this area, where global positioning system (GPS) velocities increase gradually from the northern parts towards the southern parts (Figure 1b)(McClusky et al., 2003; Reilinger et al., 2006; Kreemer et al., 2014). E-W-trending horst-graben systems are the most important neotectonic features of SW Anatolia, whereas NNW-SSE-trending basin-bounding faults are the other characteristic features of this region (Şengör, 1987; Seyitoğlu and Scott, 1992; Seyitoğlu et al., 2004; Ersoy et al., 2011; Sözbilir et al., 2011; Gürer et al., 2013). One of these active structures, the NE-dipping Yatağan Fault, bounds the SW margin of the Yatağan-Bayır Basin and continues toward NW of the Muğla city centre, where it meets the SW-dipping Muğla Fault with a complex geometry (Figure 2). GPS studies, focal mechanism solutions, and kinematic analyses of the slickensides on the fault planes have indicated that SSW-NNE-oriented extensional forces (Figure 1b) dominantly shape the tectonic evolution of this area (Barka and Reilinger, 1997; Kiratzi and Louvari, 2003; Reilinger et al., 2006; Kreemer et al., 2014; Tur et al., 2015; Elitez et al., 2016; England et al., 2016; Basmenji, 2019).

Formation of the terrestrial Yatağan-Bayır Basin began in the Early-Middle Miocene, and the geologic and geomorphologic evolution of the basin has been mainly controlled by the Yatağan Fault (Gürer and Yılmaz, 2002; Basmenji, 2019). In general, the NW-SE-trending basin is made up of 3 major stratigraphic units (Figure 3). First, the cover series of the Menderes Massif lies at the basement of the area, Miocene units then unconformably lie on the metamorphic cover units. Finally, all of the older units are overlain by Quaternary deposits (Figure 3; Becker-Platen, 1970; Atalay, 1980; Gürer and Yılmaz, 2002; Akbaş et al., 2011; Gürer et al., 2013). Previous studies have indicated that the deposition of the Miocene basin fills were controlled and disrupted by the Yatağan Fault, which demonstrates the tectonic activity of the fault since the Neogene (Gürer and Yılmaz, 2002). Overall, the Yatağan Fault differentiates Mesozoic marbles and Quaternary units, and forms a lithologic contact along its extension (Gürer and Yılmaz, 2002; Akbaş et al., 2011).

Due to the socioeconomic pattern of the area, fertile plains generated by the Yatağan Fault, and the Aegean-type climate conditions, urbanisation and population have, and continue to, grow quickly on and around the fault. Therefore, quantifying the earthquake potential and dating of past earthquakes on the Yatağan Fault were the main goals of this study, in this relatively densely populated area. Numerous historical earthquakes and destruction have been reported for this region since ~2000 BCE to present day (Ergin, 1967; Soysal et al., 1981; Papazachos et al., 1991; Guidoboni et al., 1994; Ambraseys and Jackson, 1998; Guidoboni et al., 2005; Tan et al., 2008; Karabacak, 2016; Başarır Baştürk et al., 2017). This information simply denotes that SW Anatolia has been affected by moderate to strong earthquakes during the Late Holocene. Although there have been strong effects from past earthquakes (e.g., historical damage recorded in ancient cities) in SW Anatolia, there is no clear information about the source fault and date of these events. Hence, the other primary goal of this paper was to compare known ancient earthquakes with new trench data and reveal the geochronology of these events found in the trenches in order to detect past earthquakes that generated surface ruptures.

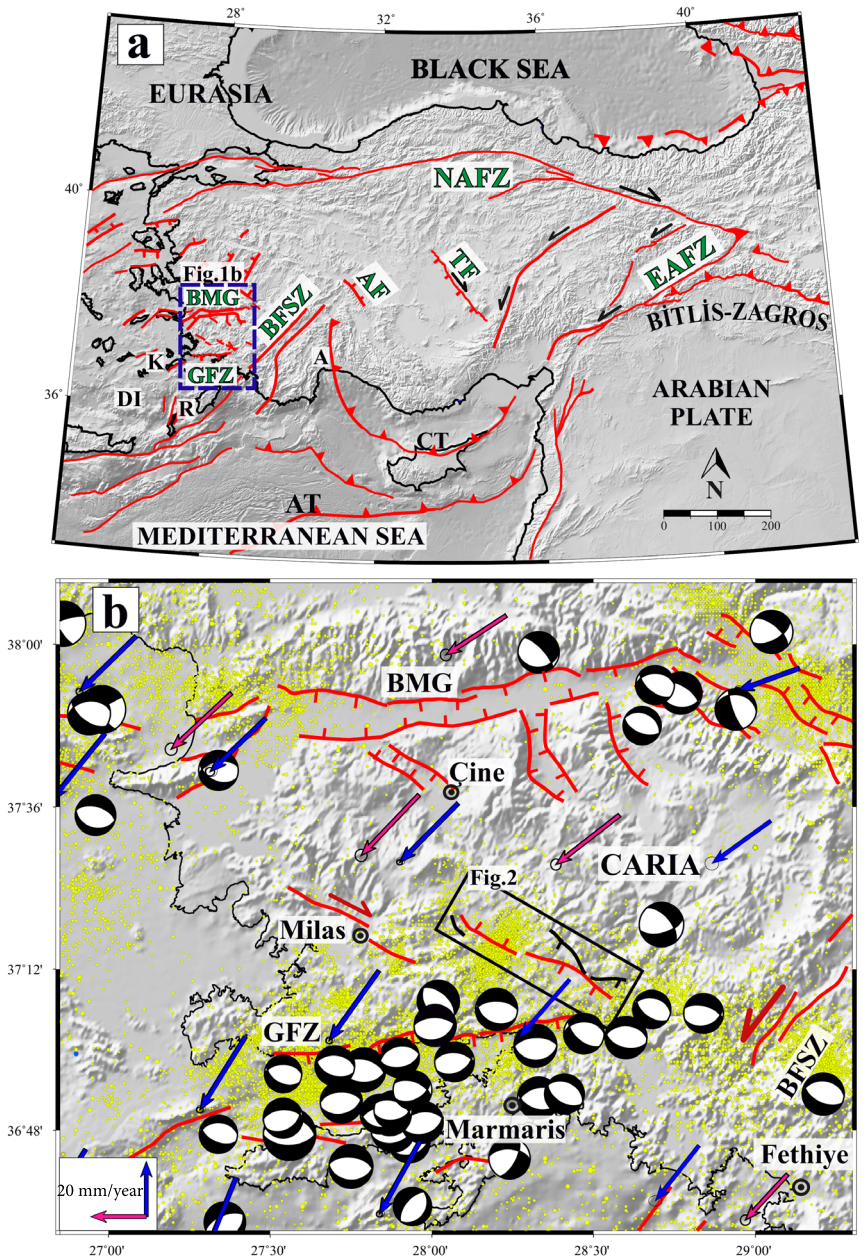

Figure 1. (a) Simplified neotectonic setting of Turkey and surrounding areas (Şengör et al., 1985, 2005, 2008, 2014; Barka, 1992; Emre et al., 2013; Hall et al., 2014). NAFZ: North Anatolian Fault Zone, EAFZ: Eastern Anatolian Fault Zone, AT: Aegean Trench, BMG: Büyük Menderes Graben, GFZ: Gökova Fault Zone, BFSZ: Burdur-Fethiye Shear Zone, CT: Cyprus Trench, AF: Akşehir Fault, TZ: Tüz Gölü Fault, DI: Dodecanese Islands, A: Antalya, K: Kos Island, R: Rhodes Island. Base map is available at GEBCO data and products (GEBCO-GBD,2019[1]). (b) Seismotectonic map of the SW Turkey (faults were from Emre et al., 2013). Small yellow circles indicate seismic activity ($M_w \geq 2.5$) between 1900 and 2020 (KOREI-EC, 2020[2]). Purple and blue arrows indicate counter-clockwise rotation with respect to Eurasia (purple arrows were from Reilinger et al., 2006; blue arrows were from England et al., 2016). Focal mechanisms downloaded from the global CMT catalogue (2020)[3] between 1965 and 2020; and compiled from Kiratzi and Louvari, 2003. The black rectangle shows the location of the Yatağan Fault. See Figure 2 for details.

[1] GEBCO-GBD(2019). Gridded Bathymetry Data [online]. Website http://www.gebco.net/data_and_products/gridded_batymetry_data/ [accessed 11 November 2019].
[2] KOREI-KEC (2020). Kandilli Earthquake Catalogue [online]. Website http://www.koeri.boun.edu.tr/sismo/zeqdb/ [accessed 03 March 2020].
[3] Global CMT Catalogue (2020). Global CMT Catalog Search [online]. Website https://www.globalcmt.org/CMTsearch.html [accessed 03March 2020].

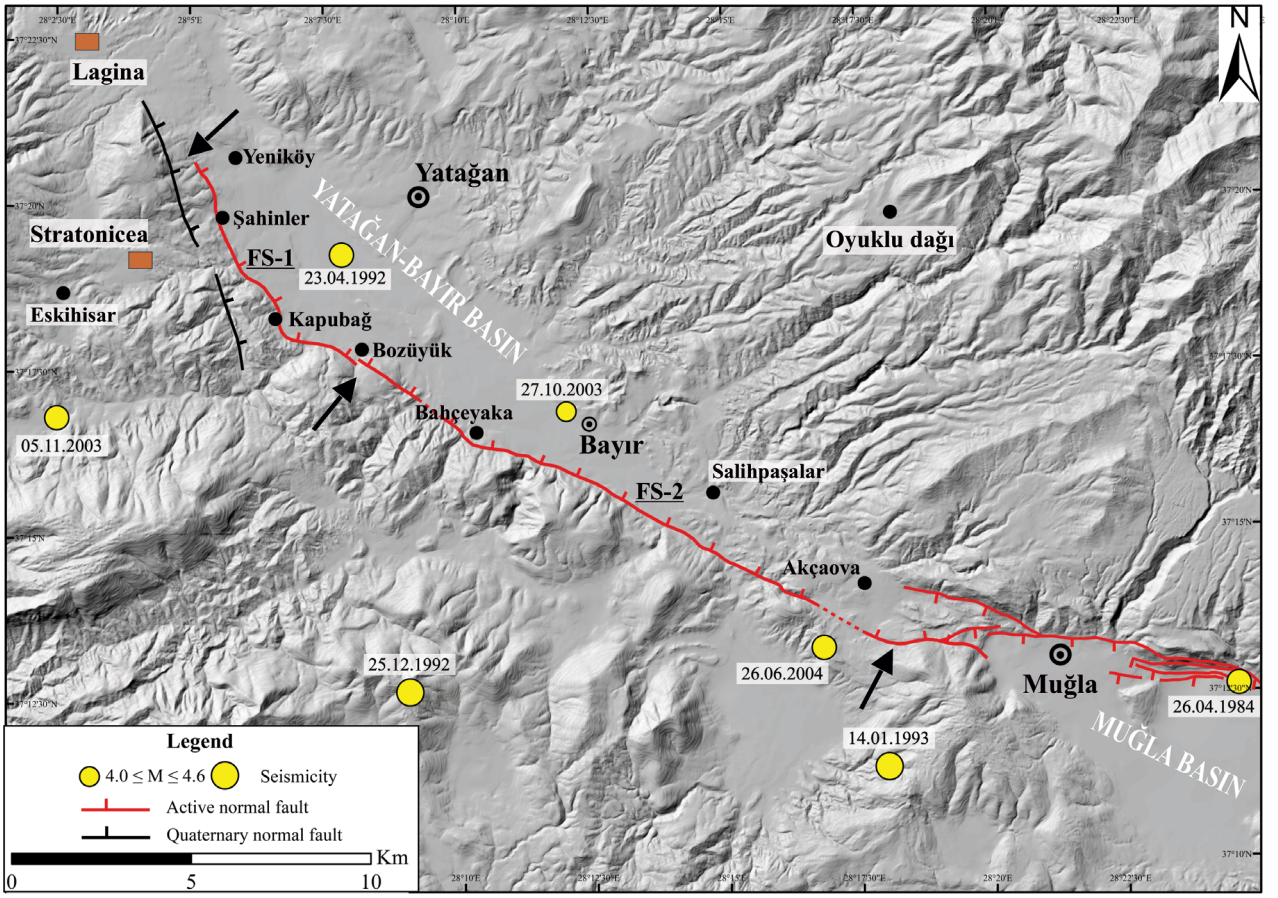

Figure 2. Geometry of the Yatağan and Muğla faults and the epicenter distribution of Mw≥4 earthquakes. Black arrows show boundaries of the fault segments (FS-1 and FS-2). Brown rectangles denote the location of ancient settlements within the study area. Black circles indicate the location of the modern cities and villages. Earthquake data was from Kadirioğlu et al. (2018); from 1965 to 2012.

2. Seismotectonic setting of the study area

2.1. The Yatağan Fault

The Yatağan Fault is one of the active structures that was generated as a result of N-S extension (Reilinger et al., 2006) between the Büyük Menderes Graben and the Gökova Fault Zone (Figure 1b). There are limited studies about the structural characteristics of the Yatağan Fault. Initially, Atalay (1980) defined the Yatağan Fault as a NE-dipping normal fault. However, Şaroğlu et al. (1987) demonstrated the Yatağan Fault as a north western extension of the Muğla-Yatağan Fault Zone, and also indicated the fault as an active dextral strike slip fault. Finally, Duman et al. (2011) and Emre et al. (2013) defined the Yatağan Fault as a NE-dipping active normal fault, which extends between the Şahinler and Salihpaşalar villages (Figure 2). Although, the reports of previous studies have indicated information about the location and geometry of the fault, they have not provided any information regarding its actual tectonic activity and seismogenic characteristics (Karabacak, 2016).

Detailed mapping of active faults is a critical issue, as it provides valuable information about the structural, lithological, and morphological evolution of tectonically active landscapes. Additionally, detailed investigation about the location, surface ruptures, fault scarps, deformation processes, and characteristics of active faults is important to evaluate earthquake potential and their relationship to other faults (McClay, 2013; Langridge et al., 2016). Hence, in order to properly understand the structural and lithologic characteristics of the Yatağan Fault, first, digital elevation model (DEM) data (generated from a 1.25000 topographic map with a 10-m contour interval) and Google Earth images were analysed in detail, and sharp topographic lineations were determined. Next, during several field campaigns using the main criteria of surface faulting definitions of McCalpin (2009) and McClay (2013), the identified abrupt morphologic lineations (e.g., fault planes and vegetation lineaments) and vertical offsets were analysed and mapped, with special attention being paid to the

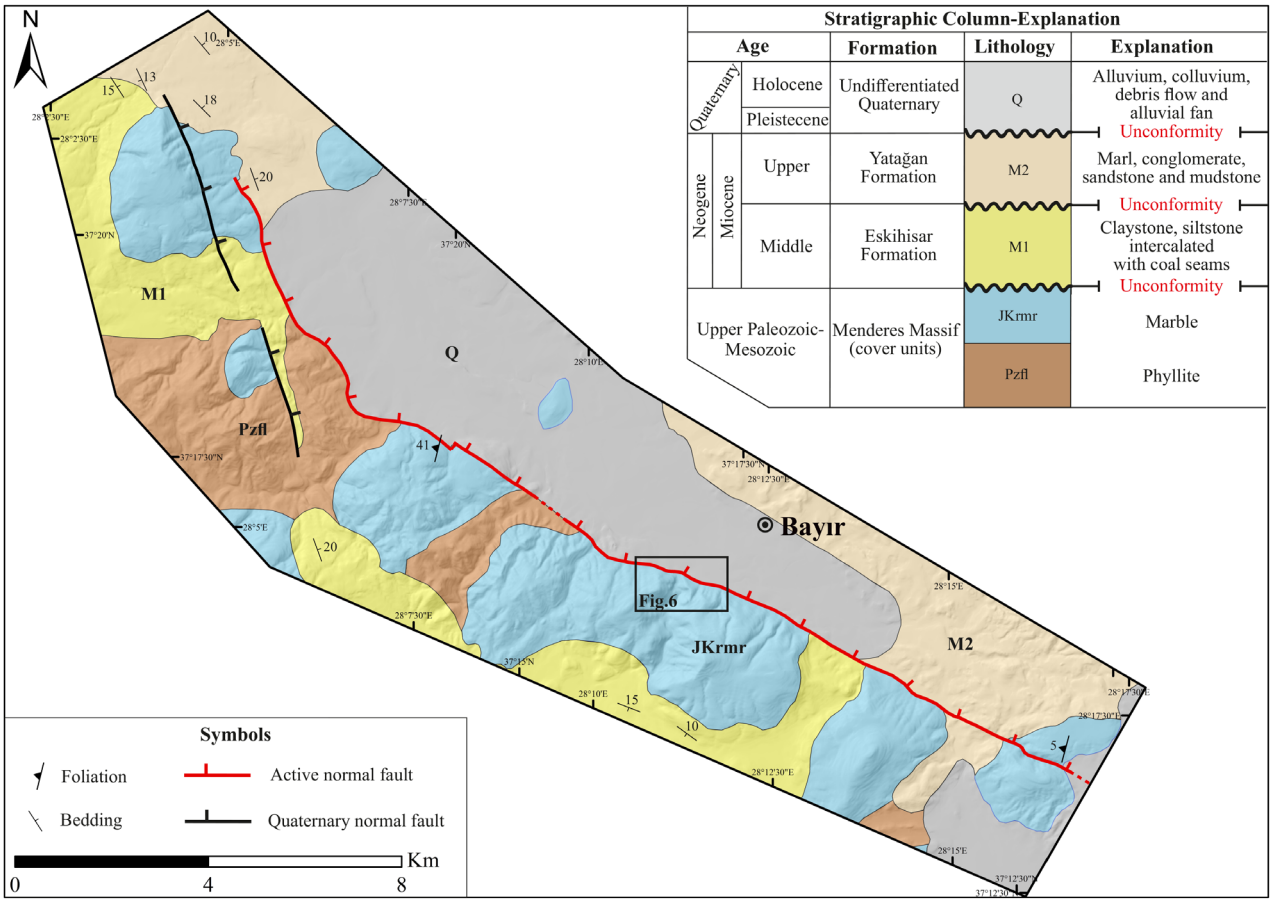

Figure 3. Geologic map and stratigraphic column of the study area (modified and compiled from Atalay, 1980; Akbaş et al., 2011; Gürer et al., 2013).

lithologic separation along the fault (stratigraphic contact between the older and younger units).

Generally, the current map of the Yatağan Fault in this study represents similar geometry to the active fault map of Duman et al. (2011) and Emre et al. (2013), but it differs significantly in the southern and northern margins of the study area. Previous studies have indicated the Yatağan Fault as single branch that is composed of several discontinuous small discrete lineations at relatively low topographic elevation. While, the field observations in this study indicated that the Yatağan Fault mostly runs through the marble formations along mountain–piedmont junction at relatively higher topographic elevation and generates a lithologic separation along its extension (Figures 2 and 3). Moreover, the area between the Şahinler and Yeniköy villages (Figure 2; at the northern margin) and the area between Salihpaşalar village and Muğla city centre (at the southern margin) was mapped for the first time herein. Furthermore, the field studies indicated that between NW of Yeniköy and western Kapubağ (at the north western part of the study area), the fault consists of 2 parallel-sub parallel branches that represent a prominent stair-step-like morphology. Overall, the extension of the fault in these locations was mainly defined by the observed marble fault scarps, topographic escarpment, and stratigraphic separation. Other observed important morphologic features of the fault were eroded fault scarps, linear mountain front, triangular facets, V-shaped valleys, fault breccia, slickensides, steep debris flows, and colluvial deposits that flow from the footwall towards the hanging wall and reflect the location, geometry, and dominant tectonic control of the Yatağan Fault on the geomorphologic processes of the basin. Assessment of the tectonic activity with morphometric indices showed considerable tectonic activity for the Yatağan Fault. In particular, triangular facet morphology based on the vertical slip rates suggested rates of 0.16 ± 0.05 and 0.3 ± 0.05 mm/year for fault segment-1 (FS-1) and FS-2, respectively as reported by Basmenji (2019).

The NW extending Yatağan Fault trends for ~30 km between Yatağan and the Muğla city center (Figure 2). The Yatağan Fault was separated into 2 geometric fault segments based on the observed certain geometric and morphologic variations [the principal criteria for segmentation of normal faults defined by McCalpin (2009) and Bull (2008)], such as mountain front geometry and change in fault orientation. Both segments (FS-1 and FS-2) form a morphologic boundary between rough and smooth topography along the mountain-piedmont junction (Figures 2 and 3), and are mainly identified by their abrupt morphological anomalies and lithological differences. Along the ~10.5-km-long FS-1, which extends between SW of Yeniköy and Kapubağ, the Yatağan Fault presents curved fault geometry and has a strike of N20–30°W in this area. To the southeast after Kapubağ village, FS-2 represents linear geometry with a strike of N50–70°W. Generally, the Yatağan Fault bounds the SW margin of the Yatağan-Bayır Basin, and generates sharp linear traces on the morphology and steep fault planes with average dip of ~80°NE (Figures 4a–4d). Field studies and structural analyses of the fault planes and slickensides on the observed fault scarps along the Yatağan Fault have indicated a normal sense of motion with a minor dextral component, which is experiencing an extension in a NNE-SSW direction (Figure 5).

Starting from the north-western margin of the study area toward the south-eastern margin, the general geometry of the Yatağan-Bayır Basin represents a wedge pattern. Between Akçaova and the Muğla city centre, the Yatağan Fault meets the Muğla Fault with a complex fault geometry through a narrow canyon. Generally, the E-W-striking fault tips here bifurcate into 2 small branches and steepen near to vertical when they pass through the northern and southern hand edges of the canyon (Figure 2). The geometry of the linking faults here is mainly influenced by the interaction between Muğla and the Yatağan Faults. Further towards the southeast, the fault enters the Muğla Basin, and runs through NW of the basin. However, in this part, the fault represents SW-dipping normal fault morphology, and is known as the Muğla Fault (Figure 2).

2.2. Historical earthquakes

The long-standing civilisation in the Muğla district provided valuable data about past seismic activity and destructive earthquakes (Tırpan and Söğüt, 2003; Ambraseys, 2009). However, there is no clear evidence about the activity of individual fault segments within the area. Several earthquake catalogues and archaeological reports were investigated in order to study the seismic activity of the Yatağan Fault in ancient times. Investigation into the reports indicated that ancient settlements in the Aegean

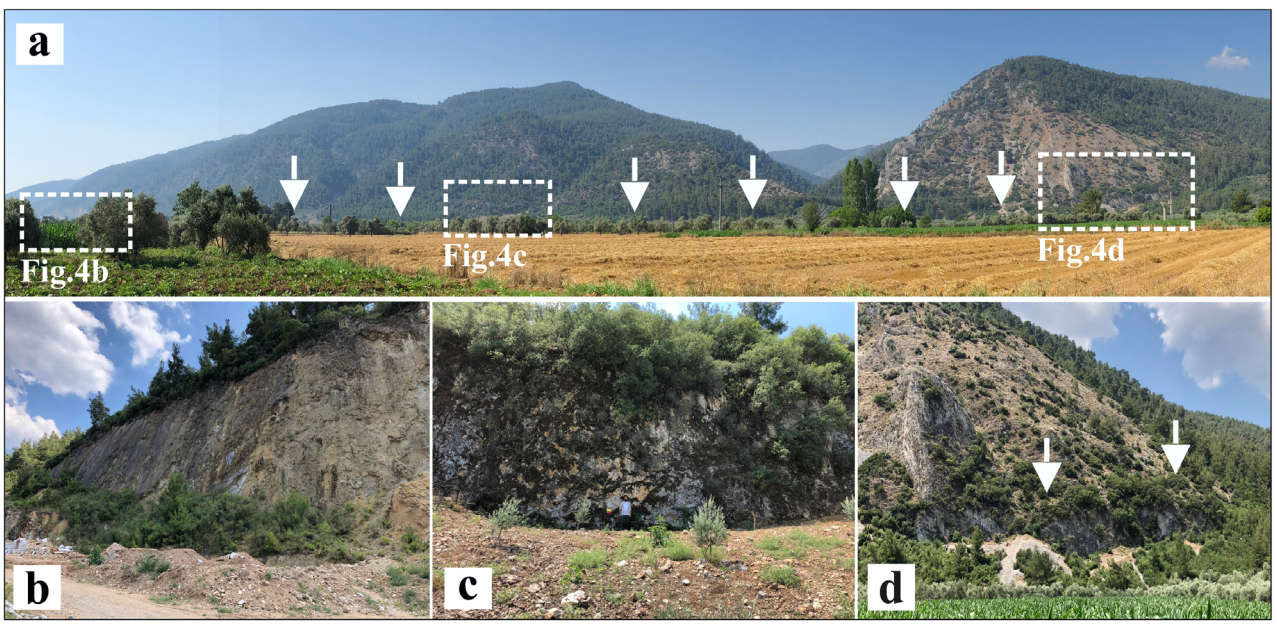

Figure 4. (a) Panoramic photograph showing the morphological features along the FS-2 segment, where the straight mountain fronts, triangular facets, and steep fault scarps are the characteristic features of the Yatağan Fault (facing west). White arrows show the location of the Yatağan Fault. (b–d) The steep (dip ~80°NE) marble fault scarps along the FS-2 segment (facing south for b and west for c and d).

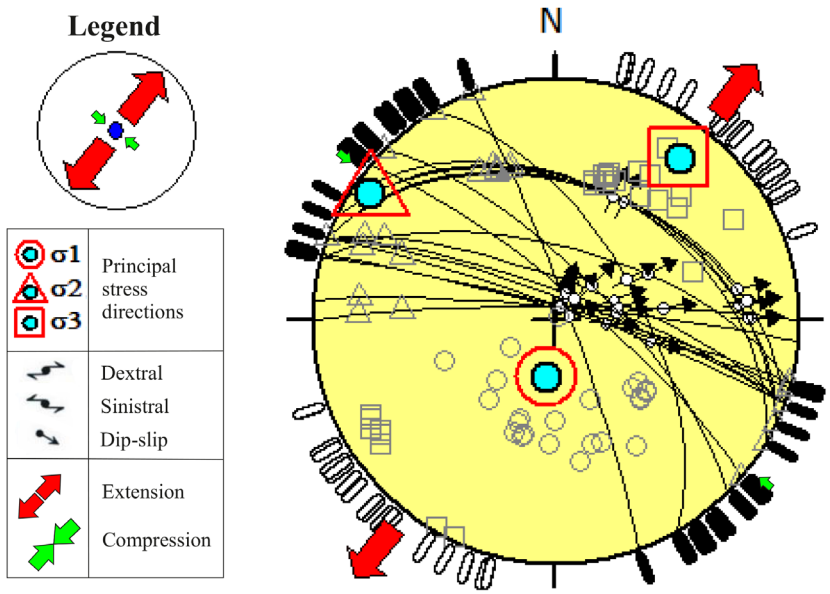

Figure 5. Principal stress axes constructed based on fault-slip data.

region were demolished several times as a result of various destructive earthquakes. Several historic earthquakes have been reported in SW Turkey since 2100 BCE (Ergin, 1967; Soysal et al., 1981; Papazachoset al., 1991; Guidoboni et al., 1994; Ambraseys and Finkel, 1995; Ambraseys and Jackson, 1998; Guidoboni et al., 2005; Tan et al., 2008; Ambraseys, 2009; Karabacak, 2016; Başarır Baştürk et al., 2017). However, their source parameters, such as the hypocenter location, depth, magnitude, and time, are ambiguous or contain uncertainties. On the other hand, there are some relatively reliable reports about the structural damage in ancient cities, state buildings, and sacred areas adjacent to the Yatağan Fault.

However, careful examination has indicated that most of the destructive earthquakes that have affected SW Anatolia were generated by the Aegean Arc-Trench System (Guidoboni et al., 1994; Guidoboni et al., 2005; Ambraseys, 2009). For example, the 1957 Rodos-Fethiye earthquake, generated by the Aegean Arc demolished several settlements and towns around the city of Yatağan, in addition to extensive destruction around the Fethiye district (Ersoy et al., 2000). After that earthquake, the town of Bayır and Eskihisar villages were moved to their present location. Therefore, it is necessary to distinguish the source of earthquakes while evaluating historical earthquake data, particularly in regions with different active faults. Historical earthquakes evaluated with this perspective are summarised in Table 1, from old to new.

142 CE Caria, Lycia and Lindus earthquake: after this violent event, lots of ancient cities in SW Turkey were badly destroyed (Table 1), and after the earthquake, Emperor Antonius donated a massive amount of money for restoration. In particular, the ancient city of Stratonicea (Figure 2; close to modern Eskihisar village, located ~2 km west of the Yatağan Fault) was extensively destroyed and received 250,000 Denarii (ancient Roman silver coin) for reconstruction, which was much more than other cities received.

4th c. CE sacred area of Lagina earthquake (~10km NW of the town of Yatağan): Archaeoseismological investigations and excavations in the sacred area of Lagina (Figure 2) suggested that the area was ruined by an earthquake in the late 4th c. CE or slightly thereafter (Table 1) (Tırpan and Söğüt, 2003; Tırpan and Büyüközer, 2012; Karabacak, 2016). During the chapel excavations, tensile cracks were observed on the walls. Moreover, it was observed that the walls were tilted from east to west (Tırpan and Söğüt, 2003). Furthermore, in the chapel excavations in 2001, according to the architectural evaluations that recovered coins and small antiques found in the chapel, it was concluded that the chapel may have been built after 325 CE. Probably in the second half of the same century, the area was abandoned after being destroyed by an earthquake (Tırpan and Söğüt, 2003). Additionally, investigations along the western part of the chapel temple indicated that the architect blocks had collapsed from northeast to

Table 1. List of historical earthquakes in and around the study area.

N	Date	Coordinate Latitude (N)-Longitude (E)	I	M	Damaged areas	Reference
1	142 CE (1, 2, 3, 5, 6, 7) or 148 CE (3, 4)	36.42–38.00 (5) or 36.70–28.00 (7)	8 (5)	7 (5)	From the Kos and Rhodes Islands to the Gulf of Antalya, to Çine, in the north, with a radius of 90 km (2,6), or to Rhodes Island (3), the Dodecanese Islands (4,7), or Caria and Dodecanese Islands (5)	(1, 2, 3, 4, 5, 6, 7)
2	4th c. CE	-	-	-	Sacred area of Lagina	(8, 9, 10)
3	Feb 1851	37.22–28.35 (11)	-	-	No damage	(6, 11)

(1) Başarır Baştürk et al., (2017); (2) Guidoboni et al., (1994); (3) Soloviev et al., (2000); (4) Papadopoulos et al., (2007); (5) TRANSFER project[1]; (6) Ambraseys, (2009); (7) NOAA data base [2]; (8) Tırpan and Söğüt, (2003); (9) Tırpan and Büyüközer, (2012); (10) Karabacak, (2016); (11) Ersoy et al., (2000).

[1] European Commission (2020). Tsunami risk and strategies for the European region (TRANSFER) Project 2009 [online]. Website https://cordis.europa.eu/project/id/37058 [accessed 23 October 2019].

[2] National Oceanic and Atmospheric Administration (NOAA) (2021). NOAA data base [online]. Website https://www.ngdc.noaa.gov/nndc/struts/results.

southwest after an earthquake (Tırpan and Söğüt, 2003). Karabacak (2016) supported this opinion as the result of observed systematic destruction in different parts of the sacred area, block rotations, orientation of collapsed columns, tilting, and age analysis of the buried material with ^{14}C and thermoluminescence (TL) dating.

Feb 1851 CE Muğla earthquake: seismic shaking was felt around Muğla and Yatağan (Table 1); however, no damage or surface ruptures were reported (Ersoy et al., 2000; Ambraseys, 2009; Başarır Baştürk et al., 2017).

2.3. Instrumental period earthquakes

The 23rd May 1941 earthquakes (Ms = 6 19:51:53 and Ms = 5.2 22:34:12): these events (Table 2) occurred with foreshocks, which destroyed 255 buildings in the Muğla city centre. While, it only slightly damaged the Oyuklu Dağı residential area and Gökova city centre. According to the literature, no ground rupture was reported for these events (Ersoy et al., 2000; Kadirioğlu et al., 2018; ISC Bulletin, 2019[1]).

The 13 December 1941 Muğla-Yatağan Earthquake (M = 6): this event resulted in a significant amount of damage in the town of Yatağan, while the Muğla, Marmaris, and Milas settlements suffered only slight damage (Ersoy et al., 2000). According to the literature, although the 1941 earthquakes did not generate any surface ruptures, and the epicentre locations given for these events were inconsistent, the town of Yatağan was greatly damaged after this event (Table 2).

Apart from these events, 6 more earthquakes of M ≥ 4 have been recorded on and around the Yatağan Fault to date (Figure 2, Table 2). However, 2 earthquake events that occurred on 23 April 1992 and 27 October 2003, at magnitudes of M_w = 4.1 and M_w = 4.0, respectively, were located on the hanging wall of the Yatağan Fault, and were in accordance with the dip angle and direction of the fault. Other seismic events were located on the western and southwestern parts of the footwall of the Yatağan Fault, and their epicentre distribution was inconsistent with the orientation and dip direction of the fault (Figure 2).

[1] ISC Bulletin (2019). Event catalogue search [online]. Website http://www.isc.ac.uk/iscbulletin/search/catalogue/ [accessed 11 November 2019].

2.4.Paleoseismic trenching

Taking into account the uncertainties regarding the earthquake history of the Yatağan Fault, paleoseismic trenching was conducted to investigate the paleoearthquake activity of the Yatağan Fault. For this study, 2 trenches were excavated at 1 site along the Yatağan Fault.

2.5. Site selection and field observations

DEM data and Google Earth images were combined with field campaigns to map the morphological trace of the active normal faulting and for site selection of the trenching. Suitable sites were selected based on fault morphology, source of sedimentation, and logistic criteria, as discussed by McCalpin (2009) and Akyüz et al. (2015).

Steeply dipping fault planes, generated by normal faulting, bound the southwestern margin of the Yatağan-Bayır Basin and differentiate the older rock units and recent sedimentary deposits (Figure 6). Therefore, digging a trench exactly in front of these fault planes was mostly delimited by thick and steep sequences of debris flows and colluvial deposits, which prevented access to the main fault plane. Hence, after careful examination, the Bahçeyaka site was selected as the trenching site.

2.6. Bahçeyaka trench site

The Bahçeyaka trench site was located at the central part of the Yatağan Fault (Figure 2; ~4km west of the town of

Table 2. List of instrumental earthquakes in the study area.

N	Date	Coordinate Latitude (N)-Longitude (E)	Time	D (km)	M	M	Reference
1	23.05.1941	37.25–28.00 (1) or 37.07–28.21 (2)	19:51:59	35 (1) or 40 (2)	Ms	6.0 (2)	(1, 2)
2	23.05.1941	37.25–28.00 (1) 37.22–28.35 (2)	23:00:48 (2)	35 (1) or 48 (2)	Ms	5.2 (2)	(1, 2)
3	13.12.1941	37.00–28.00 (2) or 37.13–28.06 (3)	6:16:05 (2)	100 (2)	Ms	6.0 (2)	(2, 3)
4	23.04.1992	37.3264–28.1395	23:11:39	11 (1) or 30.8 (2)	Mw	4.1 (2)	(1, 2)
5	25.12.1992	37.21–28.15	2:25:51	3.0	Mw	4.5	(2)
6	14.01.1993	37.19–28.30	15:24:25	21	Mw	4.6	(2)
7	27.10.2003	37.2800–28.2000	03:05:21	3 (1) or 5 (3)	Mw	3.9 (1) or 4.0 (3)	(1, 3)
8	05.11.2003	37.28–28.04	7:56:01	8.9	Mw	4.1	(2)
9	26.06.2004	37.22–28.28	6:24:00	10	Mw	4.3	(2)

(1) ISC Bulletin, (2019); (2) Kadirioğlu et al., (2018); (3) Kalafat et al., (2007); (4) Ersoy et al., (2000).

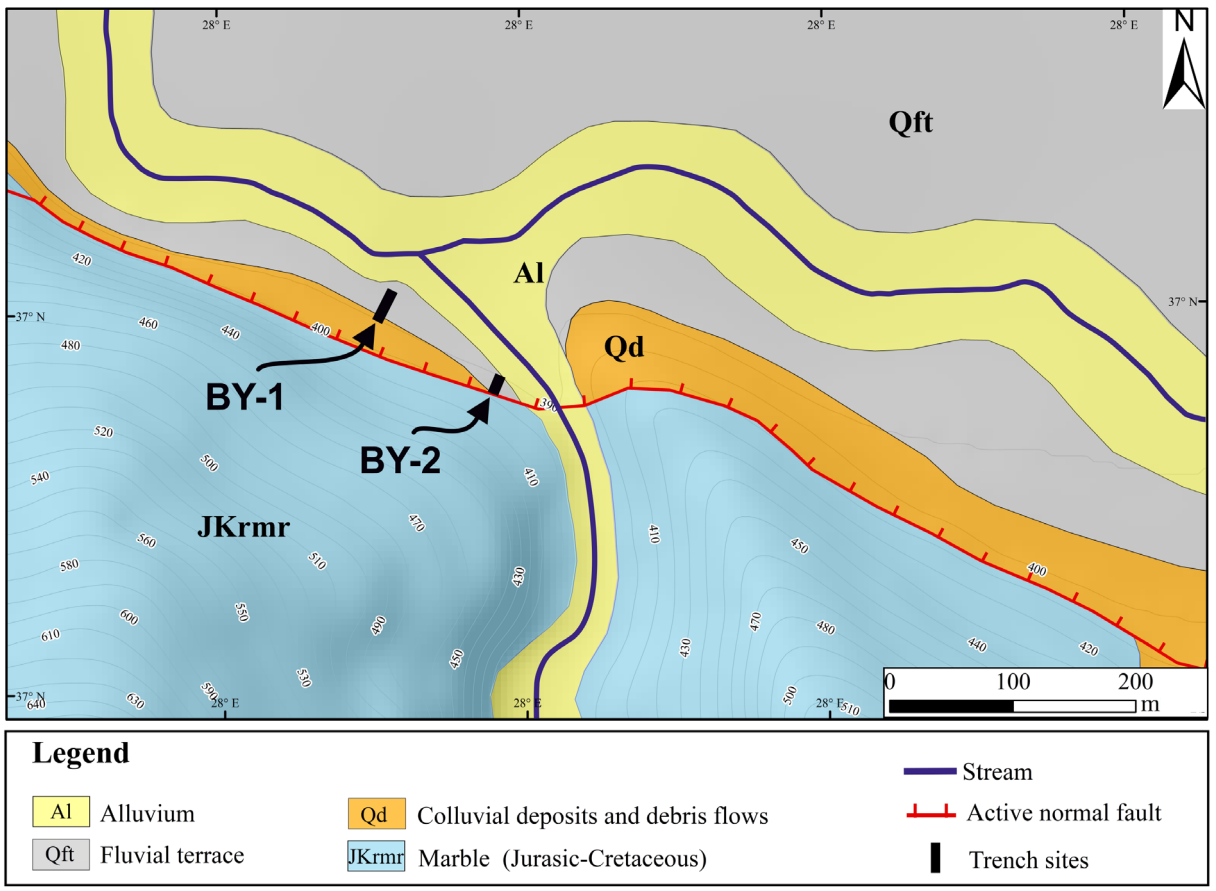

Figure 6. Geometry of the Yatağan Fault and the main geomorphological features of the Bahçeyaka trench site (contour interval 10 m; see Figure 3 for location).

Bayır). The fault in this location is represented by a dominantly normal sense of motion with a minor dextral strike-slip component. The fault strike, dip, and slickenside rake angle parameters are N70°–75°W, ~85°NE, and ~70°, respectively (Figure 5). These fault planes are the main morphotectonic features that governed the geomorphologic evolution of the area (Figures 4a–4d).

Two trenches were excavated perpendicularly to the fault strike at this location (Figure 6), comprising Bahçeyaka-1 (BY-1) and BY-2. The Bahçeyaka trench site lies on the fluvial deposits of the terrace formed by a channel branch that flows toward Yatağan Stream (Figure 6). In addition to fluvial deposits, the trench site is affected by colluvial deposits. Terrace deposits formed by the stream branch provide adequate stratigraphy and a suitable environment for sedimentation. However, as discussed above, the colluvial deposits form a topographic obstacle in front of the fault scarps, which delimits access by the excavator to those scarps (Figure 7a). As a result, the BY-1 trench was excavated perpendicularly, at 20 m north of the main fault plane. In doing so, at least the secondary structures or the antithetic faults could be exposed within the trench site. The N20°E-trending BY-1 trench was 21-m-long with an average depth of about 3 m.

Towards ~150 m SE of the BY-1 trench, where normal faulting cuts the terrace deposits, the BY-2 trench was excavated, just in front of the marble fault scarp (Figures 4 and 7b). The BY-2 trench provided favourable sedimentation and surface faulting morphology; however, due to the morphological limitations of the fluvial terrace, the trench was limited to a length of 10 m and depth of 2.5 m in a N20°E direction, perpendicular to the fault scarp.

Bahçeyaka-1 trench

The east wall of the BY-1 trench was chosen for log preparation and sampling. The trench stratigraphy reflected an abundance of fluvial deposits over colluvial deposits. Fluvial sediments, which formed the lower unit of the trench wall, showed a fining upward pattern with pebbles/cobbles in a sandy matrix (Unit I; Figure 8). In the southwestern part of the trench, angular pebbles and

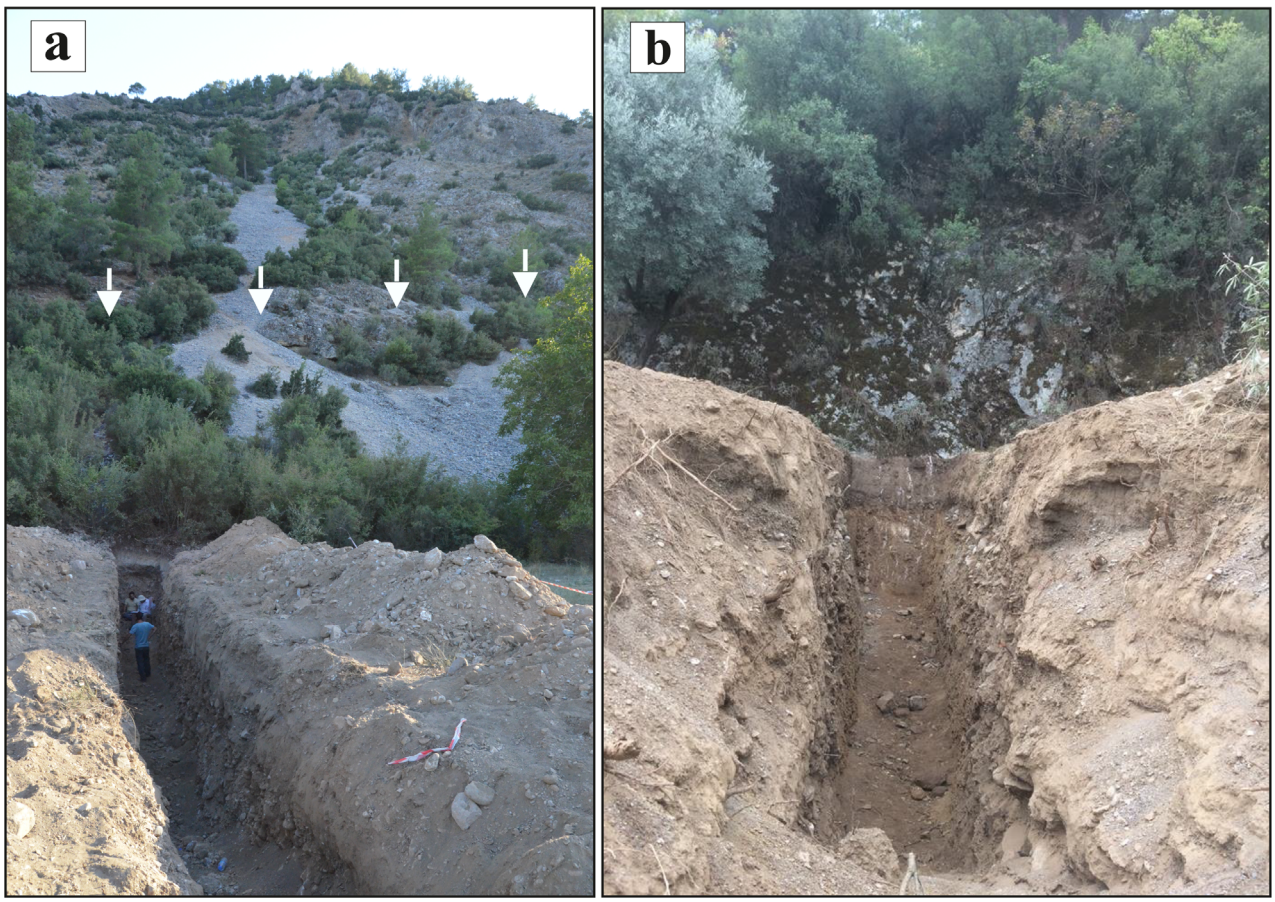

Figure 7. General view of: (a) BY-1 trench (white arrows indicate the marble fault scarp). (b) BY-2 trench (marble fault scarp in the background; both facing SW).

cobbles, in a sandy/silty matrix, overlayed Unit I, with a wedge geometry (Unit II). In particular, the beige sandy silty unit showed fining upward; however, angular blocks could also be seen in patches. This unit was covered by 2 sediment packages with lateral and horizontal geometry (Units III and IV). Wedge-shaped sequences with colluvial deposits (Unit III) made up of angular pebbles in a sandy/silty matrix, extended from the southernmost tip of the trench to 17 m, thinned out, and overlapped Unit VII (Figure 8). This sedimentary package was characterised by the increasing matrix rate from the base towards the top. Furthermore, this sedimentary layer reflected a high-energy sediment flux from the footwall block of the fault. Unit IV revealed fluvial sediments made up of angular pebble/cobbles in a sandy/silty matrix, which must have been deposited after an erosional process. This sedimentary package, with a complex geometry, was characterised by angular limestone pebbles and blocks. In the southwestern part of the trench, beige sandy silt with angular blocks (Unit VII; average diameter of a block ~30 cm) overlies Unit IV and displays fining upward. Whereas, toward the northeast of the trench, light brown sands with silt and cobbles overlies Unit IV.

In the north eastern part (at 3 m) of the trench, fluvial deposits of the lower unit included vertically oriented tabular pebbles with respect to the other horizontally oriented within the sedimentary package, which marked an antithetic fault (Figures 8 and 9). This secondary fault was located inversely to the main fault plane, with a high dip angle of ~80–85°. The antithetic fault cut Units I and V (light brown silt with blocks), and was capped by yellow silt with sand pebble intercalations (Unit VIII).

The lower boundary of Units VII and VIII was defined as the event horizon (the white line in Figure 8) in the BY-1 trench. In order to determine the age range of this earthquake event, 3 radiocarbons and 3 optically-stimulated luminescence (OSL) samples were taken from the lower and upper limits of the event layer (Tables 3 and 4). To limit the age range of the earthquake event above the event horizon, 2 OSL samples were collected from the yellow silty unit (Unit VIII). Whereas, 3 ^{14}C samples and 1 OSL sample (Tables 1 and 2) represented the lower boundary of the event horizon. In order to restrict the time interval of the event horizon, the lower boundary of the event level was delimited by the BY1-B3 radiocarbon sample (Unit VI), whereas the upper limit was bounded by the BY1-OSL1 sample (Unit VII). This boundary condition indicated an earthquake event that took place before 1054 ± 84 CE, and after 366–160 BCE (93.9%-2σ probability).

Bahçeyaka-2 trench

The BY-2 trench was opened on the same fluvial terrace, formed by a channel branch that flowed towards Yatağan Stream (Figure 6). The channel branch was the main factor that controlled the sedimentation at this site. Based on that fact, the trench exposures indicated fluvial sediments with a negligible amount of colluvial deposits. In this area, the main fault scarp bounded the SW edge of the BY-2 trench (Figure 7b). Since this trench was dug right in front of the fault plane, the structural elements observed in the BY-2 trench were more prominent when compared to those in the BY-1 trench. Similar to the BY-1 trench, the east wall of the BY-2 trench was chosen for logging.

The oldest stratigraphic level in the trench was a small package of pebbles and cobbles in a sandy matrix (Unit

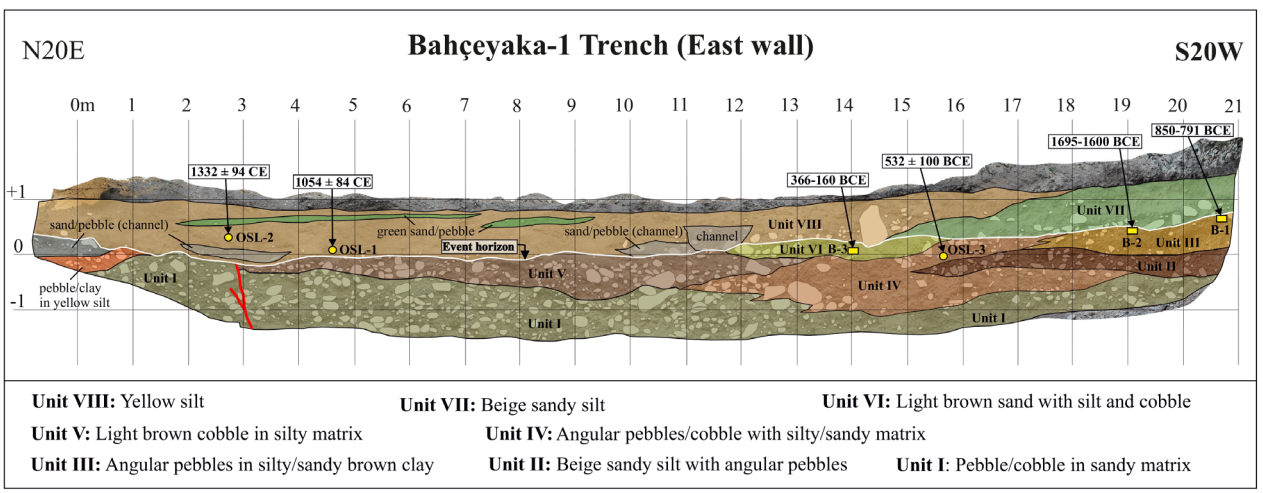

Figure 8. Photomosaic and log of the BY-1 trench. See Figure 6 for the trench location.

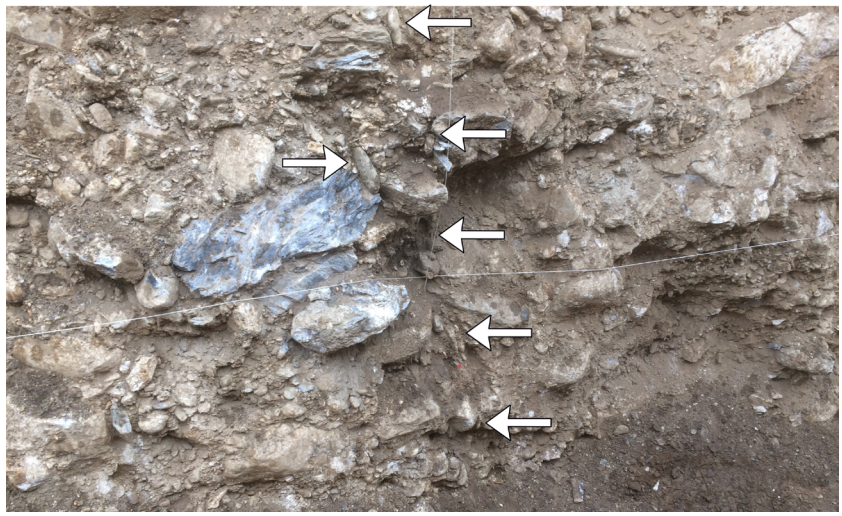

Figure 9. Close-up view of the antithetic fault seen at 3rd m in the BY-1 trench.

Table 3. Radiocarbon samples of BY-1 and BY-2 trenches and probability of events determined using Oxcal 4.3.2 (Ramsey, 2017).

Sample number	Lab code	Material type and weight (mg)	Radiocarbon age(BP)	2 sigma calibration
BY1-B1	Poz-102947	Charcoal 0.2 mg	2650 ± 30 BP	895–869 BCE (5.9%) 850–791 BCE (89.5%)
BY1-B2	Poz-109421	Charcoal 0.3 mg	3350 ± 30 BP	1737–1715 BCE (5.4%) 1695–1600 BCE (76.8%) 1586–1534 BCE (13.2%)
BY1-B3	Poz-102786	Charcoal 0.2 mg	2180 ± 35 BP	132–118 BCE (1.5%) 366–160 BCE (93.9%)
BY2-B1	Poz-102782	Charcoal 0.5 mg	150 ± 30 BP	1667–1709 CE (16.3%) 1717–1784 CE (31.4%) 1796–1890 CE(30.0%) 1910–1938 CE (17.7%)
BY2-B2	Poz-102866	Charcoal 0.05 mg	9090 ± 110 BP	8609–8161 BCE (82.2%) 8150–7966 BCE (13.2%)
BY2-B3	Poz-102784	Charcoal 0.4 mg	2740 ± 35 BP	975–954 BCE (4.5%) 944–812 BCE (95.4%)

I; Figure 10). This layer was overlain by angular pebbles/cobbles and gravels within brown clay (Unit II). This unit was cut by 2 main fault zones; one was just in front of the exposed fault surface (sheared reddish-brown clay), and the other extended between 4.5 and 5.5 m of the trench (oxidised, shared green clay; Figures 10, 11a, and 11b). These structures were located parallel-subparallel to the main fault plane and reflected traces of the last major earthquake on the Yatağan Fault. Unit II was capped by poorly-sorted, well-rounded blocks and pebbles within a clay-silt matrix (Unit III). Different fluvial and channel deposits lay above this sediment package. The channel deposits were characterised by a thin gravel band in a greyish sandy matrix. Finally, fine gravel and silt in a sandy matrix (Unit V) covered all of the older units after an erosional period, and the most distinctive feature of this unit was the greyish sand with the thin gravel bands.

The lower boundary of the Unit III represented the event horizon in this trench (the white line in Figure 10). In order to determine the age range of the last major earthquake on the Yatağan Fault, a total of 3 radiocarbons and 3 OSL samples (Tables 3 and 4) were collected from

Table 4. BY-1 and BY-2 trench OSL dating results.

Sample number	K (%)[a]	U (ppm)[a]	Th (ppm)[a]	Cosmic dr[b]	De CAM (Gy)[c]	De MAM (Gy)[d]	Environmental dose rate (gray/ka)	Age (ka)	Chronological age
BY1-OSL1	1.37	2.16	8.38	0.175	2.3 ± 0.2	1.98 ± 0.27	2.39 ± 0.02	0.964 ± 0.084	1054 ± 84 CE
BY1-OSL2	1.75	2.46	9.92	0.175	2.1 ± 0.2	1.51 ± 0.21	2.89 ± 0.03	0.686 ± 0.094	1332 ± 94CE
BY1-OSL3	2.18	4.42	16.85	0.176	10.5 ± 0.4	10.4 ± 0.64	4.12 ± 0.04	2.55 ± 0.1	532 ± 100BCE
BY2-OSL1	1.59	2.33	8.17	0.197	4.6 ± 0.2	4.4 ± 0.34	2.63 ± 0.03	1.676 ± 0.131	342 ± 131CE
BY2-OSL2	1.61	2.38	7.99	0.165	3.9 ± 0.4	2.82 ± 0.35	2.61 ± 0.03	1.08 ± 0.134	938 ± 134CE
BY2-OSL3	1.68	2.35	8.22	0.168	3.7 ± 0.2	3.04 ± 0.33	2.69 ± 0.03	1.132 ± 0.123	886 ± 123CE

[a] Analyses obtained using laboratory gamma spectrometry.
[b] Dose response curve.
[c] Dose equivalent central age model using Galbraith and Roberts (2012).
[d] Dose equivalent minimum age model.

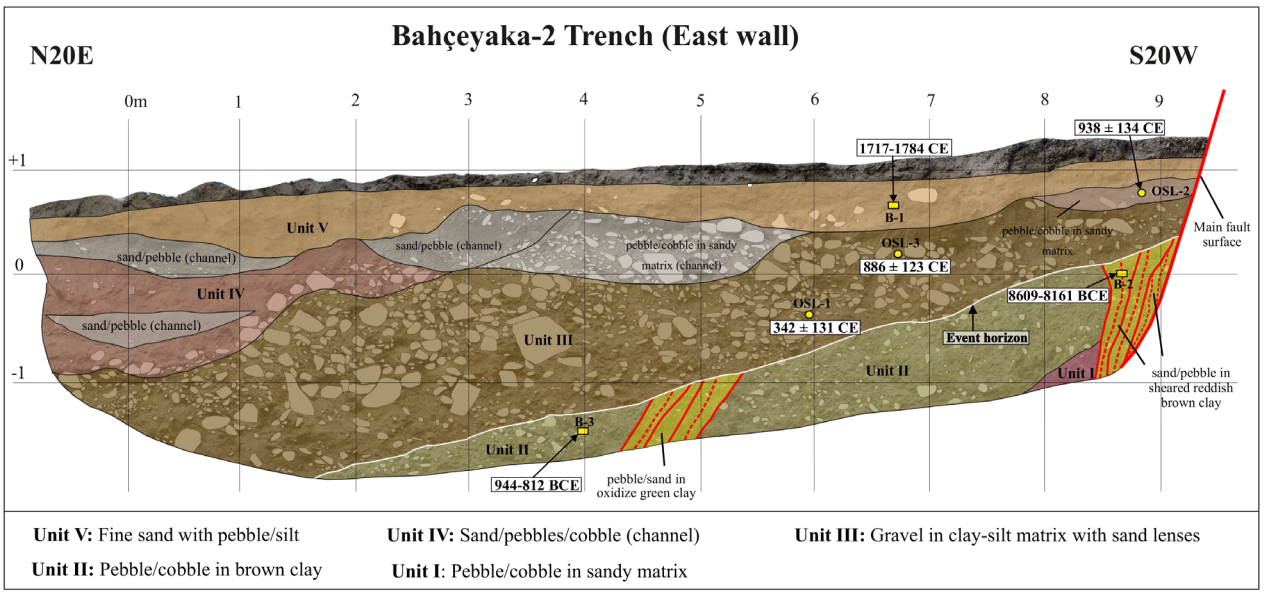

Figure 10. Photomosaic and log of the BY-2 trench (See Figure 6 for trench location).

above and below the event horizon. Two ^{14}C samples were taken from Unit II, comprising 1 from inside of the shear zone and 1 from the upper parts of the sedimentary package. Furthermore, 1 ^{14}C sample and 3 OSL samples were taken from the units that covered the fault structure (units above the event horizon). Generally, the age ranges of the dated samples in the BY2 trench were consistent with each other.

In order to define the time interval of the major earthquake event, the BY2-B3 and BY2-OSL1 samples were chosen as the lower- and upper-boundaries of the event horizon (Figure 10). Accordingly, an earthquake event with a surface rupture was constrained between 878 ± 65 BCE and 944–812 BCE (95.4%-2σ probability).

Combined interpretation of trench studies

Paleoseismic investigations on the structural and stratigraphic features of the BY-1 and BY-2 trenches indicated an earthquake event. In order to define the time interval of this earthquake, a total of 6 radiocarbons and 6 OSL samples were dated from the upper and lower boundaries of the event horizon (Tables 3 and4). In the BY-1 trench, the upper part of the event horizon was delimited by the BY1-

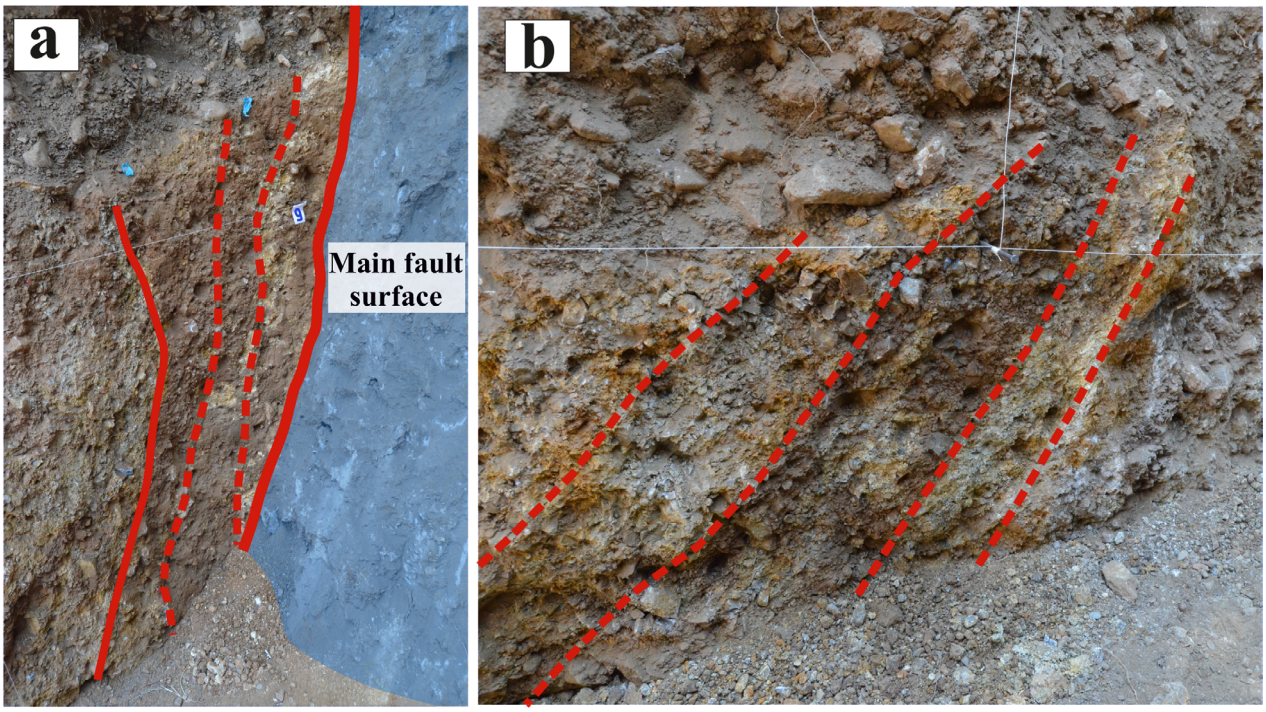

Figure 11. Close-up view of fault zones at 9 (a) and 5 (b) m in the BY-2 trench.

OSL1 and BY1-OSL2 samples (Figure 8), while the lower boundary was dated by different sediment packages with samples BY1-B1, BY1-B2, BY1-B3, and BY1-OSL3. In the BY-2 trench, the BY2-OSL-1, BY2-OSL-2, BY3-OSL-3, and BY2-B-1 samples were taken from the upper units of the event horizon (Figure 10), whereas the BY2-B-2 and BY2-B-3 samples represented the lower units. The OSL samples were prepared at the Sakarya University MALTA Laboratory, then dated at the Ankara University Nuclear Sciences Institute Laboratories. Radiocarbon samples were dated at the Poznan Radiocarbon Laboratory using accelerator mass spectrometry. Furthermore, the ^{14}C samples were calibrated using OxCal v.4.3.2 (Ramsey, 2017), which utilised the IntCal13 atmospheric curve of Reimer et al. (2013).

Based on the dating results, separate time intervals were defined for each of the recognised paleo-earthquakes in the trenches. Generally, the results were consistent with the trench stratigraphy and with each other. The event horizon of the paleo earthquake detected in the BY-1 trench was limited by the BY1-B3 sample from below and the BY1-OSL1 sample from above (Figure 8). These samples indicated a time range between 366 and 160 BCE (93.9%-2σ probability) and 1054 ± 84 BC. Another earthquake event was defined in the BY-2 trench, and this event horizon was limited by the BY2-B3 sample from below and the BY2-OSL1 sample from above (Figure 10). Radiocarbon dating yielded a time range between 944 and 812 BCE (95.4%-2σ probability) and 342 ± 131 BC.

The stratigraphic sequence relationship and dating results for both of the trenches seemed to be consistent with each other, and delimited the time range of the single earthquake event from above and below. It was important to limit the event horizon with the lower boundary of the BY-1 trench and the upper boundary of the BY-2 trench (Figures 8 and 10). This boundary condition restricted the timespan to a relatively narrower interval. Integrated interpretation of the trench data indicated an earthquake event that had ruptured the surface between 366 and 160 BCE (93.9%-2σ probability) and 342 ± 131 BC.

3. Discussion and conclusion

Detailed morphologic, structural, and stratigraphic investigations were conducted along the Yatağan Fault and combined with paleoseismology studies to assess the earthquake activity of the fault during the Late Quaterna-

ry. Field observations indicated that the NW-SE-trending Yatağan Fault predominantly shaped the geologic and geomorphologic evolution of the area. The analysed kinematic indicators (e.g., slickensides) on the fault scarps indicated an almost pure normal sense of motion with a minor right lateral strike slip component, as the result of NE-SW extension. Field studies and the DEM data analysis revealed that the Yatağan Fault generated sharp linear traces on the topography. The performed tectonic geomorphology assessments of Basmenji (2019) yielded notable tectonic activity for the Yatağan fault, and emphasised the effective control of the fault on the geomorphic features of the area, and suggested triangular facet slope angle-based vertical slip rates of 0.16 ± 0.05 mm/year and 0.3 ± 0.05 mm/year, for the FS-1 and FS-2, respectively. Additionally, consistent with the calculated uplift rates, the normalised channel steepness (k_{sn}) investigation along the Yatağan Fault suggested moderate to high channel steepness changes across the mountain front of the footwall block (Basmenji, 2019). The combination of the results indicated a remarkable vertical uplift along the Yatağan Fault. The tectonic geomorphology investigations simply indicated the tectonic activity of the Yatağan Fault and its potential to generate moderate earthquakes. Furthermore, in order to assess the maximum earthquake magnitude (MAG) of the Yatağan Fault using quantitative methods, the Wells and Coppersmith (1994) empirical method for normal fault generated ruptures (MAG = 1.32 × LOG (RL) + 4.86, where RL represents the rupture length) was applied. Based on the mapped fault length (~30 km), the calculation suggested a MAG of 6.6 for the fault if FS-1 and FS-2 rupture together. A comparison of the calculated magnitude for the Yatağan Fault with well-studied recent earthquakes that have generated surface ruptures, their rupture length, characteristics, and slip rates associated with normal faults, such as the Dinar and Akşehir Faults in neighbouring regions, allowed for a more in-depth discussion of the estimated hypothetical magnitude. The Dinar earthquake (M = 6.1) generated an ~10 km-long surface rupture and 50-cm vertical offset (Altunel et al., 1999). Furthermore, a 3.50-m vertical displacement has been observed over the last 3500 years as a result of the 3 earthquake events (including the 1995 event), which suggested a 0.1-mm/year vertical slip rate along the fault (Altunel et al., 1999). Thus, the recurrence period of large earthquakes is 1500–2000 years (Altunel et al., 1999). Additionally, a paleoseismological investigation of the 2002 Çay earthquake (M_w = 6.2) rupture yielded a 25–30-cm vertical offset and ~5.5-km-long ground rupture (Akyüz et al., 2006). Moreover, the tectonic geomorphology investigations yielded a vertical slip rate of 0.1 mm/year for the Çay segment (Topal et al., 2016). Overall, an investigation through the well-studied normal faults in western Anatolia and neighbouring regions has indicated that normal faults with a similar slip rate of 0.1–0.3 mm/year can generate moderate earthquakes every few thousand years (Altunel et al., 1999; Topal et al., 2016).

In terms of the threshold value of coseismic surface ruptures, the minimum magnitude required to a generate surface rupture with normal faulting was previously proposed by Bonilla (1988) and DePolo (1994), using a relatively similar data set of earthquake records and empirical methods. They suggested magnitudes of M_L or M_w 5.5 and M_w 6.3–6.5. Similarly, historical earthquake data collection with various magnitudes by Wells and Coppersmith (1994) and Stirling et al. (2002) indicated that even a shallow earthquake, with $M_w \leq 5$, was not capable of rupturing the ground surface (McCalpin, 2009). As ground motions of earthquakes bellow $M_w = 5$ are barely strong enough to generate observable geologic evidence, such as surface faulting, liquefaction, or landslides (Jibson and Keefer, 1993; McCalpin, 2009), the threshold value (M_L or M_w 5.5) of Bonilla (1988) is a favourable choice for the lower boundary of ground ruptures generated by normal faults (McCalpin, 2009). However, on a local scale, knowledge and data related to the observation of the threshold of surface ruptures along normal faults in SW Anatolia is very limited, but since the relationship between the moment magnitude, surface rupture length, and vertical throw rates are proportional (Altunel et al., 1999; McCalpin, 2009), these parameters from previous studies can provide valuable insight and relevant analogues. In the Mediterranean region, ground ruptures produced by relatively small normal faults were heavily influenced by several $M_W \geq 6$ earthquakes, such as the 30 October 2016 earthquake, with Mw = 6.6 or 6.5, on the Mont Vettore Fault in central Italy (Villani and Sapia, 2017; Galli et al., 2019); 23 November 1980 earthquake, with M_S = 6.9, on the Irpina Fault in southern Italy (Pantosti et al., 1993); 5 February 1783 earthquake, with M > 7, on the Cittanova Fault in southern Italy (Galli and Bosi, 2002); 6 October 1964 earthquake, with M_S = 6.9, on the Salur segment of the Manyas Fault in northwest Turkey (Kürçer et al., 2017); 1 October 1995 earthquake, with M = 6.1, on the Dinar Fault, in SW Turkey (Altunel et al., 1999); and 3 February 2002 earthquake, with M_w = 6.2, on the Çay segment of the Akşehir Fault in western Turkey (Akyüz et al., 2006). These studies have shown that even the smallest earthquake events with magnitudes of M = 6.1 or M_w = 6.2 were capable of producing 50-cm and 25–30-cm vertical offset on the Dinar Fault and Akşehir Fault, respectively (Altunel et al., 1999; Akyüz et al., 2006). Therefore, as previously suggested by Bonilla (1988), and compiled from the mentioned previous studies on normal faults in the Mediterranean region, a threshold value of Mw ≥ 5.5 would be a good choice for the minimum threshold ratio value along the Yatağan fault. This finding also exhibits good agreement with the criteria of McCal-

pin (2009), based on observations of paleo earthquakes in terms of the moment magnitude ratio and distribution of the paleoseismic evidence (e.g., surface faulting).

In order to study the unknown earthquake history of the Yatağan Fault and assess the vertical slip rates associated with past events, paleoseismological trenching was performed for the first time along the fault. A total of 6 radiocarbon and 6 OSL samples were compiled from the BY-1 and BY-2 trenches. The dating results were consistent with each other and could be matched between the 2 trenches (Tables 3 and 4). However, the BY2-B2 sample, which was taken from the inner parts of the shear zone, close to main fault exposure, gave an irrelevant age (probably reworked), which was not consistent with the other dating results and stratigraphy (Table3), most probably due to the transportation of the organic material, through erosional processes, from another location to the fault zone, or due to insufficient organic material. Hence, this sample was not considered during the interpretation of the age ranges of the earthquake event. The dating results of the collected samples and interpretation of the trench stratigraphy and structural elements indicated the existence of at least 1 paleoearthquake, which was detected in the BY-1 trench and yielded a time span from 366–160 BCE (93.9%-2σ calibration probability) to 1054 ± 84 CE (Figure 8; Tables 3 and 4). Another event was defined in the BY-2 trench, which implied a time interval between 944 and 812 BCE (95.4%-2σ calibration probability) and 342 ± 131 CE (Figure 10; Tables 3 and 4). The results from both trenches were consistent with each other and limited the event horizon from below and above. In order to constrain the timing of the latest earthquake event observed in the trenches, the compiled ^{14}C and OSL dates from the BY-1 and BY-2 trenches were combined. It was critical to restrict the timeframe of the recognised events in both trenches with the BY1-B3 sample (lower boundary of the event horizon in the BY-1 trench) and BY2-OSL2 sample (the upper boundary of event horizon in the BY-2 trench; Figure 12). Correlation of the boundary conditions related to the event horizons of both trenches suggested a paleoearthquake that produced surface ruptures between 366 and 160 BCE (93.9%-2σ probability) and 342 ± 131 CE.

On the other hand, although the main evidence of ground rupturing during the last earthquake event (documented structural evidence in both trench walls clearly indicated a coseismic surface rupture) was found, with regards to the coseismic vertical throw measurement, due to the high-energy sediment flux (chaotic) along the steep marble fault planes, a lack of favourable sediment horizons, the discontinuity of the stratigraphic layers, and abundance of certain reference stratigraphic units, which implied vertical displacement along the fault (fault slip data) the possibility of cumulative and/or individual offset measurements associated with the earthquake event identified in the trenches is surely undermined. However, as discussed by Altunel et al. (1999), the active normal faults in southwestern Anatolia are capable of generating a considerable amount of coseismic vertical displacement during 1 event [for example the 20 September 1899 Menderes earthquake was associated with ~2 m of vertical throw; Ambraseys and Finkel, (1987)].

Earthquake catalogues and different sources have proposed 2 earthquake events, which have provided relatively reliable information about damaged ancient settlements around the Yatağan Fault (Guidoboni et al., 1994; Tırpan and Söğüt, 2003; Ambraseys, 2009; Tırpan and Büyüközer, 2012; Karabacak, 2016). An earthquake affected the SW parts of Turkey and the Dodecanese Islands in 142 CE. This earthquake affected an area with an approximate radius of 90km, from the Kos and Rhodes Islands to the Gulf of Antalya and Çine in the north (Figures 1a and 1b), which caused considerable damage at various levels in the ancient settlements. After this destructive event, many ancient cities in SW Turkey received funding for reconstruction and restoration (Guidoboni et al., 1994; Ambraseys, 2009). Even though the timing and location of this earthquake is controversial, according to Guidoboni et al. (1994) and Ambraseys (2009), it was emphasised that the ancient city of Stratonicea (located 2 km west of the Yatağan Fault) (Figure 2) was heavily damaged and received more funding for reconstruction than the other ancient cities in the Caria region (Figure 1b) (Guidoboni et al., 1994; Ambraseys, 2009). Although the ancient city of Stratonicea was located adjacent to the Yatağan Fault, the damage pattern of the 142 CE event and tsunami reports (Ambraseys, 2009) associated with this event should also be considered. Therefore, it is unlikely that this event can be correlated with the geochronologically constrained time span obtained from the trench studies.

The sacred area of Lagina is located ~8km NE of the ancient city of Stratonicea. The sacred area was joined to the ancient city of Stratonicea during second half of the 3rd c. CE (Büyüközer, 2010; Ekici, 2010; Karabacak, 2016). The area presents well-preserved ruins; thus, coordinated archaeological investigations since 1993 in this area have provided valuable information about historical earthquakes and associated fault characteristics (Karabacak, 2016). Archaeoseismological investigations in the sacred area have suggested a systematic deformation and dislocation pattern throughout the area, especially along the buildings, walls, and columns (Tırpan and Söğüt, 2003; Karabacak, 2016). Collapse and orientation of the columns in a parallel pattern, tilting of stairs and walls, block rotations and folding on the ground are systematic, and implied an earthquake event in the late 4th c. CE (Tırpan and Söğüt, 2003; Tırpan and Büyüközer, 2012; Karabacak,

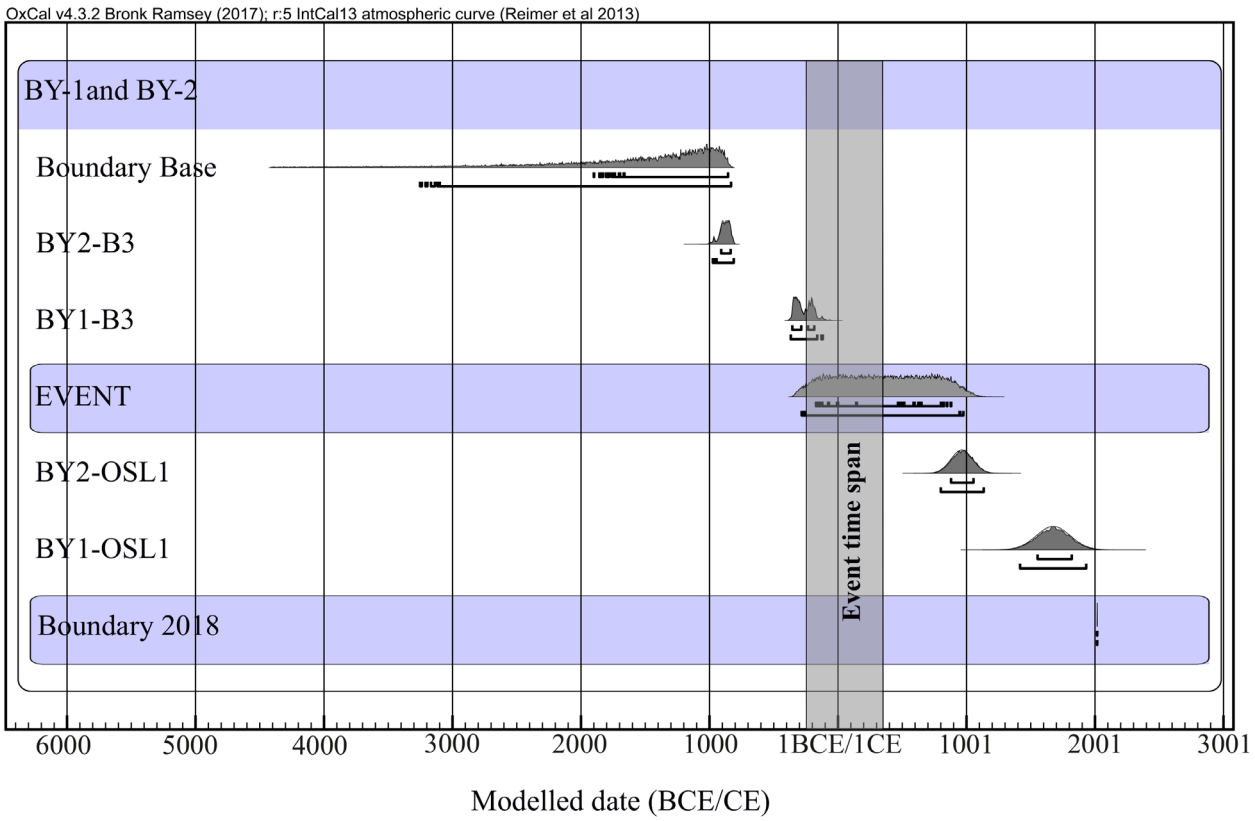

Figure 12. The graph shows the identified event in the BY-1 and BY-2 trenches with respect to probability of the radiocarbon ages and OSL dating distribution (Ramsey and Lee, 2013). Under each curve, the range limit represents a probability of 68.2% and 95.4%, respectively.

2016). Furthermore, the orientation of the deformation and dilations in the area were consistent with the geometry and framework of the Yatağan Fault, which supported the archaeoseismological investigations, and geological and morphological studies (Karabacak, 2016). Additionally, the TL and ^{14}C dating methods were applied to assess the age of the buried depositions and ceramic items, which yielded an age that was consistent with the proposed earthquake event. The trench studies and field observations indicated a good match with the archaeoseismological records and observed systematic deformation. Therefore, a surface rupturing earthquake event between 366 and 160 BCE (93.9%-2σ probability) and 342 ± 131 CE, from the BY-1 and BY-2 trenches, can be correlated with the earthquake event in the 4th c. CE.

In summary, detailed geological, geomorphological, and paleoseismological investigations along the Yatağan Fault suggested notable seismic hazard potential for the study area. While, growing population and civilisation in the area is another concern. Overall, the combination of trench data and morphology-derived slip rates (Basmenji, 2019) with well-studied recent earthquakes and surface ruptures along the normal faults have shown that the Yatağan Fault has the potential to generate moderate earthquakes with relatively long intervals. Comprehensive interpretation of the trench data with other earthquake activities on the neighbouring active faults will emphasise the earthquake potential of the Yatağan Fault in the future.

Acknowledgments

This study is a chapter of the MSc thesis of Mehran Basmenji, which was funded by the Scientific and Technological Research Council of Turkey (TÜBİTAK; Project No: 116Y179). The authors acknowledge the enthusiastic financial and moral support of Dr. Marjan Basmenji during the studies. We thank Dr. Cengiz Zabcı and Dr. Aynur Dikbaş for their critical comments and suggestions. We are grateful to Prof. Dr. Semih Ergintav and Prof. Dr. Cenk Yaltırak for their advice and fruitful discussions. We are thankful to Dr. Korhan Erturaç, Dr. Eren Şahiner, and Dr. Niyazi Meriç with regards to the OSL dating, and also to Enver Sürmeli and Beste Karatepe for their assistance during the trench studies. We would like to thank 2 anonymous reviewers for their constructive feedback and comments, which improved the first version of the manuscript. Some figures in this paper were generated using Generic Mapping Tools (Wessel et al., 2013).

References

Adamia SA, Chkhotua T, Kekelia M, Lordkipanidze M, Shavishvili I et al. (1981). Tectonics of the Caucasus and adjoining regions: implications for the evolution of the Tethys ocean. Journal of Structural Geology 3 (4): 437-447. doi: 10.1016/0191-8141(81)90043-2.

Akbaş B, Akdeniz N, Aksay A, Altun İ, Balcı V et al. (2011). Türkiye Jeoloji Haritası. Maden Tetkik ve Arama Genel Müdürlüğü Yayını. Ankara, Turkey: Maden Tetkik ve Arama Genel Müdürlüğü (in Turkish).

Aktug B, Ozener H, Dogru A, Sabuncu A, Turgut B et al. (2016). Slip rates and seismic potential on the East Anatolian Fault System using an improved GPS velocity field. Journal of Geodynamics 94: 1-12.

Akyüz HS, Uçarkuş G, Şatır D, Dikbaş A, Kozacı Ö (2006). 3 Şubat 2002 Çay depreminde meydana gelen yüzeykırığı üzerinde paleosismolojik araştırmalar. Yerbilimleri Dergisi 27 (1): 41-52 (in Turkish).

Akyüz HS, Karabacak V, Zabcı C (2015). Paleoseismic trenching. In: Beer M, Kougioumtzoglou IA, Patelli E, Au SK (editors). Encyclopedia of Earthquake Engineering. 1st ed. Heidelberg, Germany: Springer, pp. 1779-1792.

Allen M, Jackson J, Walker R (2004). Late Cenozoic reorganization of the Arabia-Eurasia collision and the comparison of short-term and long-term deformation rates. Tectonics 23 (2). doi: 10.1029/2003TC001530

Altunel E, Barka A, Akyüz S (1999). Palaeoseismicity of the Dinar Fault, SW Turkey. Terra Nova 11 (6): 297-302.

Ambraseys N (editor) (2009). Earthquakes in the Mediterranean and Middle East: a multidisciplinary study of seismicity up to 1900. 1st ed. Cambridge, UK: Cambridge University Press.

Ambraseys NN, Finkel CF (1987). Seismicity of Turkey and neighbouring regions, 1899-1915. Annales Geophysicae 5 (6): 701-725.

Ambraseys NN, Jackson JA (1998). Faulting associated with historical and recent earthquakes in the Eastern Mediterranean region. Geophysical Journal International 133 (2): 390-406.

Ambraseys NN, Finkel CF (editors) (1995). Seismicity of Turkey and Adjacent Areas: A Historical Review, 1500-1800. 1st ed. Virginia, USA: MS Eren.

Atalay Z (1980). Stratigraphy of continental Neogene in the region of Muğla-Yatağan, Turkey. Geological Bulletin of Turkey 23: 93-99.

Barka AA (1992). The north Anatolian fault zone. Annales Tectonicae 6: 164-195.

Barka A, Reilinger R (1997). Active tectonics of the Eastern Mediterranean region: deduced from GPS, neotectonic and seismicity data. Annals of Geophysics XL (1997): 587-610. doi: 10.4401/ag-3892

Başarır Baştürk N, Özel NM, Altınok Y, Duman TY (2017). Türkiye ve yakın çevresi için geliştirilmiş tarihsel dönem (MÖ 2000-MS 1900-) deprem kataloğu. In: Duman TY (editor). Türkiye Sismotektonik Haritası Açıklama Kitabı. Ankara, Turkey: Maden Tetkik ve Arama Genel Müdürlüğü, pp. 34-239 (in Turkish).

Basmenji M (2019). Yatağan Fayı'nın paleosismolojik ve morfotektonik özellikleri (Muğla, GB Türkiye). MSc, İstanbul Technical University, İstanbul, Turkey (in Turkish).

Becker-Platen JD (1970). Lithostratigraphische Untersuchungen im Kanozoikom-Sudwest-Anatoliens (Türkei).-(Kanozoikum und Braunkohlen der Türkei. 2.). Schweizerbart'sche Verlagsbuchhandlung (in German).

Bonilla MG (1988). Minimum earthquake magnitude associated with coseismic surface faulting. Bulletin of the Association of Engineering Geologists 25 (1): 17-29.

Bozkurt E (2001). Neotectonics of Turkey-a synthesis. Geodinamica Acta 14 (1-3): 3-30.

Bull WB (editor) (2008). Tectonic geomorphology of mountains: a new approach to paleoseismology. 1st ed. New Jersey, USA: John Wiley & Sons.

Burc Oral M, Reilinger RE, Nafi Toksöz M, King RW, Barka AA et al. (1995). Global positioning system offers evidence of plate motions in eastern Mediterranean. Eos Trans 76 (2): 9-11.

Büyüközer A (2010). Lagina Hekate Tapınağı'nın altyapı ve Stylobat düzenlemesinde uygulanan oranlar. Pamukkale Üniversitesi Sosyal Bilimler Enstitüsü Dergisi (7): 1-13 (in Turkish).

DeMets C, Gordon RG, Argus DF, Stein S (1990). Current plate motions. Geophysical Journal International 101 (2): 425-478.

DePolo CM (1994). The maximum background earthquake for the Basin and Range Province, western North America. Bulletin of the Seismological Society of America 84 (2): 466-472.

Duman TY, Emre Ö, Özalp S, Elmacı H (2011). 1: 250,000 scale active fault map series of Turkey, Aydın (NJ 35-11) Quadrangle. General Directorate of Mineral Reserach and Exploration Publications. Ankara, Turkey: General Directorate of Mineral Research and Exploration.

Ekici M, (2010). Lagina kutsal alanında bulunan sikkelerin değerlendirilmesi. Pamukkale Üniversitesi Sosyal Bilimler Enstitüsü Dergisi 7: 31-38 (in Turkish).

Elitez İ, Yaltırak C, Aktuğ B (2016). Extensional and compressional regime driven left-lateral shear in southwestern Anatolia (eastern Mediterranean): The Burdur-Fethiye Shear Zone. Tectonophysics 668 (2016): 26-35.

Emre Ö, Duman TY, Özalp S, Elmacı H, Olgun Ş et al. (2013). Açıklamalı Türkiye Diri Fay Haritası Ölçek 1/1.125.000. Maden Tetkik ve Arama Genel Müdürlüğü Yayını. Ankara, Turkey: Maden Tetkik ve Arama Genel Müdürlüğü (in Turkish).

England P, Houseman G, Nocquet J (2016). Constraints from GPS measurements on the dynamics of deformation in Anatolia and the Aegean. Journal of Geophysical Research 121 (12): 8888-8916.

Ergin K (editor) (1967). A catalogue of earthquakes for Turkey and surrounding area (11AD to 1964AD). 1st ed. İstanbul, Turkey: ITU Earth Physics Institute Publications.

Ersoy Ş, Altınok Y, Yalçıner AC (2000). Güneybatı Anadolu'nun Neotektonik Yapılarına Genel bir bakış ve bölgenin deprem etkinliği. In: III. Ulusal Kıyı Mühendisliği Sempozyumu; Çanakkale, Turkey.

Ersoy YE, Helvacı C, Palmer MR (2011). Stratigraphic, structural and geochemical features of the NE–SW trending Neogene volcano-sedimentary basins in western Anatolia: implications for associations of supra-detachment and transtensional strike-slip basin formation in extensional tectonic setting. Journal of Asian Earth Sciences 41 (2): 159-183.

Galadini F, Galli P (2003). Paleoseismology of silent faults in the Central Apennines (Italy): the Mt. Vettore and Laga Mts. faults. Annals of Geophysics 46 (5): 815-836.

Galbraith RF, Roberts RG (2012). Statistical aspects of equivalent dose and error calculation and display in OSL dating: an overview and some recommendations. Quaternary Geochronology 11 (2012): 1-27.

Galli P, Galderisi A, Peronace E, Giaccio B, Hajdas I et al. (2019). The awakening of the dormant Mount Vettore fault (2016 central Italy earthquake, Mw 6.6): paleoseismic clues on its millennial silences. Tectonics 38 (2): 687-705.

Galli P,Bosi V (2002). Paleoseismology along the Cittanova fault: implications for seismotectonics and earthquake recurrence in Calabria (southern Italy). Journal of Geophysical Research 107 (B3): ETG-1.

Guidoboni E, Comastri A, Traina G, Geofisica RIN (editors) (1994). Catalogue of Ancient Earthquakes in the Mediterranean Area up to the 10th Century. 1st ed. Rome, Italy: Istituto Nazionale di Geofisica e Vulcanologia.

Guidoboni E, Comastri A, Boschi E (2005). The exceptional earthquake of 3 January 1117 in the Verona area (northern Italy): a critical time review and detection of two lost earthquakes (lower Germany and Tuscany). Journal of Geophysical Research 110: B12309.

Gürer ÖF, Sanğu E, Özburan M, Gürbüz A, Sarica-Filoreau N (2013). Complex basin evolution in the Gökova Gulf region: implications on the Late Cenozoic tectonics of southwest Turkey. International Journal of Earth Sciences 102 (8): 2199-2221.

Gürer ÖF, Yılmaz Y (2002). Geology of the Ören and surrounding regions, SW Turkey. Turkish Journal of Earth Sciences 11: 2-18.

Hall J, Aksu AE, Elitez I, Yaltırak C, Çifçi G (2014). The Fethiye–Burdur Fault Zone: a component of upper plate extension of the subduction transform edge propagator fault linking Hellenic and Cyprus Arcs, Eastern Mediterranean. Tectonophysics 635:80-99.

Jibson RW, Keefer DK (1993). Analysis of the seismic origin of landslides: examples from the New Madrid seismic zone. Geological Society of America 105 (4): 521-536.

Kadirioğlu FT, Kartal RF, Kılıç T, Kalafat D, Duman TY et al. (2018). An improved earthquake catalogue (M ≥ 4.0) for Turkey and its near vicinity (19002012). Bulletin of Earthquake Engineering 16 (8): 3317-3338.

Kalafat D, Güneş Y, Kara M, Deniz P, Kekovalı K et al. (2007). Bütünleştirilmiş Homojen Türkiye Deprem Kataloğu (1900-2005; M≥4.0). Kandilli Rasathanesi ve Deprem Araştırma Enstitüsü Deprem Kataloğu. İstanbul, Turkey: Boğaziçi Üniversitesi Yayınları.

Karabacak V (2016). Seismic damage in the Lagina sacred area on the Mugla Fault: a key point for the understanding of the obliquely situated faults of western Anatolia. Journal of Seismology 20 (1): 277-289.

Kiratzi A, Louvari E (2003). Focal mechanisms of shallow earthquakes in the Aegean Sea and the surrounding lands determined by waveform modelling: a new database. Journal of Geodynamics 36 (1-2): 251-274.

Kreemer C, Blewitt G, Klein EC (2014). A geodetic plate motion and Global Strain Rate Model. Geochemistry, Geophysics, Geosystems 15 (10): 3849-3889.

Kürçer A, Özaksoy V, Özalp S, Güldoğan ÇU, Özdemir E et al. (2017). The Manyas fault zone (southern Marmara region, NW Turkey): active tectonics and paleoseismology. Geodinamica Acta 29 (1): 42-61.

Langridge RM, Ries WF, Litchfield NJ, Villamor P, Van Dissen RJ et al. (2016). The New Zealand active faults database. New Zealand Journal of Geology and Geophysics 59 (1): 86-96.

McCalpin JP (editor) (2009). Paleoseismology. 1st ed. Crestone, USA: Academic Press.

McCalpin JP, Hart EW (2002). Ridge-top spreading features and relationship to earthquakes, San Gabriel Mountains region, Southern California-Part B: Paleoseismic investigations of ridge-top depressions. Final Technical Report. California, USA: National Earthquake.

McClay KR (editor) (2013). The mapping of geological structures. 1st ed. New Jersey, USA: John Wiley & Sons.

McClusky S, Balassanian S, Barka A, Demir C, Ergintav S et al. (2000). Global Positioning System constraints on plate kinematics and dynamics in the eastern Mediterranean and Caucasus. Journal of Geophysical Research 105 (B3): 5695-5719.

McClusky S, Reilinger R, Mahmoud S, Ben Sari D, Tealeb A (2003). GPS constraints on Africa (Nubia) and Arabia plate motions, Geophysical Journal International 155 (1): 126-138.

McKenzie D (1972). Active tectonics of the Mediterranean region. Geophysical Journal International 30 (2): 109-185.

McKenzie D (1978). Active tectonics of the Alpine-Himalayan belt: the Aegean Sea and surrounding regions. Geophysical Journal International 55 (1): 217-254.

Özkaymak Ç, Sözbilir H, Uzel B, Akyüz HS (2011). Geological and palaeoseismological evidence for late Pleistocene-Holocene activity on the Manisa Fault Zone, western Anatolia. Turkish Journal of Earth Sciences 20 (4): 449-474.

Pantosti D, Schwartz DP, Valensise G (1993). Paleoseismology along the 1980 surface rupture of the Irpinia fault: implications for earthquake recurrence in the southern Apennines, Italy. Journal of Geophysical Research 98 (B4): 6561-6577.

Papadopoulos GA, Daskalaki E, Fokaefs A, Giraleas N (2007). Tsunami hazards in the Eastern Mediterranean: strong earthquakes and tsunamis in the East Hellenic Arc and Trench system. Natural Hazards and Earth System Sciences 4 (3): 57-64.

Papazachos B, Kiratzi A, Papadimitriou E (1991). Regional focal mechanisms for earthquakes in the Aegean area. In: Udias A, Buforn E (editors). Source Mechanism and Seismotectonics. Basel, Switzerland: Springer, pp. 405-420.

Le Pichon X, Chamot-Rooke N, Lallemant S, Noomen R, Veis G (1995). Geodetic determination of the kinematics of central Greece with respect to Europe: implications for eastern Mediterranean tectonics. Journal of Geophysical Research 100 (B7): 12675-12690.

Le Pichon X, Angelier J (1979). The Hellenic arc and trench system: a key to the neotectonic evolution of the eastern Mediterranean area. Tectonophysics 60 (1-2): 1-42.

Radbruch-Hall DH (1978). Gravitational creep of rock masses on slopes. In: Voight B (editor). 1st ed. Developments in Geotechnical Engineering. Amsterdam, the Netherlands: Elsevier, pp. 607-657.

Ramsey CB (2017). Methods for summarizing radiocarbon datasets, Radiocarbon. Cambridge University Press 59 (6): 1809-1833.

Ramsey CB, Lee S (2013). Recent and planned developments of the program OxCal, Radiocarbon. Cambridge University Press 55 (2): 720-730.

Reilinger R, McClusky S, Vernant P, Lawrence S, Ergintav S et al. (2006). GPS constraints on continental deformation in the Africa-Arabia-Eurasia continental collision zone and implications for the dynamics of plate interactions. Journal of Geophysical Research 111 (B5): B05411.

Reilinger RE, McClusky SC, Oral MB, King RW, Toksoz MN et al. (1997). Global Positioning System measurements of present-day crustal movements in the Arabia-Africa-Eurasia plate collision zone. Journal of Geophysical Research 102 (B5): 9983-9999.

Reimer PJ, Bard E, Bayliss A, Beck JW, Blackwell PG et al. (2013). IntCal13 and Marine13 radiocarbon age calibration curves 0–50,000 years cal BP, Radiocarbon. Cambridge University Press 55 (4): 1869-1887.

Saroglu F, Boray A, Emre O (1987). Active faults of Turkey, General Directorate of the Mineral Research and Exploration.General Directorate of Mineral Research and Exploration Publications. Ankara, Turkey: General Directorate of Mineral Research and Exploration.

Şengör AMC (editor) (1980). Türkiye'nin neotektoniğinin esasları. Ankara, Turkey: Türkiye Jeoloji Kurumu (in Turkish).

Şengör AMC (1987). Cross-faults and differential stretching of hanging walls in regions of low-angle normal faulting: examples from western Turkey. Geological Society of London 28 (1): 575-589.

Şengör AMC, Görür N, Şaroğlu F (1985). Strike-slip faulting and related basin formation in zones of tectonic escape: Turkey as a case study. In: Biddle KT, Christie-Blick N (editors). Strike-Slip Deformation, Basin Formation, and Sedimentation, 1st ed. Texas, USA: Special Publications of SEPM, pp. 227-264.

Şengör AMC, Kidd WSF (1979). Post-collisional tectonics of the Turkish-Iranian plateau and a comparison with Tibet. Tectonophysics 55 (3-4): 361376.

Şengör AMC, Yilmaz Y (1981). Tethyan evolution of Turkey: a plate tectonic approach. Tectonophysics 75(3-4): 181-241.

Seyitoğlu G, Esat K, Kaypak B, Toori M, Aktuğ B (2019). Internal deformation of Turkish–Iranian Plateau in the hinterland of Bitlis–Zagros Suture Zone. In: Saein AF (editor). Developments in Structural Geology and Tectonics. 1st ed. Amsterdam, Netherlands: Elsevier, pp. 161-244.

Seyitoğlu G, Esat K, Kaypak B (2017). The neotectonics of southeast Turkey, northern Syria, and Iraq: the internal structure of the Southeast Anatolian Wedge and its relationship with recent earthquakes. Turkish Journal of Earth Sciences 26 (2): 105-126.

Seyitoğlu G, Işık V, Cemen I (2004). Complete Tertiary exhumation history of the Menderes massif, western Turkey: an alternative working hypothesis. Terra Nova 16 (6): 358-364.

Seyitoğlu G, Scott BC (1992). The age of the Büyük Menderes graben (west Turkey) and its tectonic implications. Cambridge University Press 129 (2): 239-242.

Soloviev SL, Solovieva ON, Go CN, Kim KS, Shchetnikov NA et al. (2000). Main Tsunamigenic Zones in the Mediterranean Sea. In: Bonnin J, Levin BW, Tinti S, Papadopoulos GA (editors). Tsunamis in the Mediterranean Sea 2000 B.C.–2000 A.D. Dordrecht, Netherlands: Springer, pp. 1-15.

Soysal H, Sipahioğlu S, Kolçak D, Altınok Y (editors) (1981). Historical earthquake catalogue of Turkey and surrounding area (2100 BC–1900 AD). 1st ed. İstanbul, Turkey: ITU Earth Physics Institute Publications.

Sözbilir H, Sarı B, Uzel B, Sümer Ö, Akkiraz S (2011). Tectonic implications of transtensional supradetachment basin development in an extension-parallel transfer zone: the Kocaçay Basin, Western Anatolia, Turkey. Basin Research 23 (4): 423-448.

Stirling M, Rhoades D, Berryman K (2002). Comparison of earthquake scaling relations derived from data of the instrumental and preinstrumental era. Bulletin of the Seismological Society of America 92 (2): 812-830.

Şengör AMC, Tüysüz O, İmren C, Sakınç M, Eyidoğan H et al. (2005). The North Anatolian fault: a new look. Annual Review of Earth and Planetary Sciences 33: 37-112.

Şengör AMC, Özeren MS, Keskin M, Sakınç M, Özbakır AD et al. (2008). Eastern Turkish high plateau as a small Turkic-type orogen: Implications for post-collisional crust-forming processes in Turkic-type orogens. Earth-Science Reviews 90 (1-2):1-48.

Şengör AMC, Grall C, İmren C, Le Pichon X, Görür N et al. (2014). The geometry of the North Anatolian transform fault in the Sea of Marmara and its temporal evolution: implications for the development of intracontinental transform faults. Canadian Journal of Earth Sciences 51(3):222-42.

Tan O, Tapirdamaz MC, Yörük A (2008). The earthquake catalogues for Turkey. Turkish Journal of Earth Sciences 17 (2): 405-418.

Tırpan A, Söğüt B (2003). Yatağan-Eskihisar Ocağı Börükçü Mevkisi 2003 Yılı Çalışmaları Raporu, Lagina Kazısı Başkanlığı, Muğla.

Tırpan AA, Büyüközer ZG (2012). The Temple of Hekate at Lagina. Architectural History and Archaeological Research 12: 181-202.

Topal S, Keller E, Bufe A, Koçyiğit A (2016). Tectonic geomorphology of a large normal fault: Akşehir fault, SW Turkey. Geomorphology 259: 55-69.

Tsodoulos IM, Stamoulis K, Caputo R, Koukouvelas I, Chatzipetros A et al. (2016). Middle–Late Holocene earthquake history of the Gyrtoni Fault, Central Greece: insight from optically stimulated luminescence (OSL) dating and paleoseismology. Tectonophysics 687: 14-27.

Tur H, Yaltırak C, Elitez İ, Sarıkavak KT (2015). Pliocene–Quaternary tectonic evolution of the Gulf of Gökova, southwest Turkey. Tectonophysics 638: 158-176.

Varnes DJ, Radbruch-Hall DH, Savage WZ (1989). Topographic and structural conditions in areas of gravitational spreading of ridges in the western United States. United States Geological Survey Professional Papers. Washington, USA: United States Geological Survey.

Villani F, Sapia V (2017). The shallow structure of a surface-rupturing fault in unconsolidated deposits from multi-scale electrical resistivity data: the 30 October 2016 Mw 6.5 central Italy earthquake case study. Tectonophysics 717: 628-644.

Wessel P, Smith WHF, Scharroo R, Luis J, Wobbe F (2013). Generic mapping tools: improved version released. Eos Trans 94(45): 409-410.